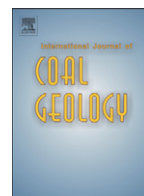




Contents lists available at ScienceDirect

## International Journal of Coal Geology

journal homepage: [www.elsevier.com/locate/ijcoalgeo](http://www.elsevier.com/locate/ijcoalgeo)

## Radiation- and self-ignition induced alterations of Permian uraniferous coal from the abandoned Novátor mine waste dump (Czech Republic)

Ivana Sýkorová<sup>a,\*</sup>, Bohdan Kříbek<sup>b</sup>, Martina Havelcová<sup>a</sup>, Vladimír Machovič<sup>a,c</sup>, Alexandra Špaldoňová<sup>a</sup>, Ladislav Lapčák<sup>c</sup>, Ilja Kněsl<sup>b</sup>, Jaroslav Blažek<sup>a</sup>

<sup>a</sup> Institute of Rock Structure and Mechanics, AS CR, v.v.i., V Holešovičkách 41, 182 09 Prague, Czech Republic

<sup>b</sup> Czech Geological Survey, Klárov 3, 118 21 Prague, Czech Republic

<sup>c</sup> University of Chemistry and Technology Prague, Technická 5, 166 28 Prague, Czech Republic

## ARTICLE INFO

## Article history:

Received 11 April 2016

Received in revised form 13 July 2016

Accepted 3 August 2016

Available online xxx

## Keywords:

Coal wastes

Organic matter

Uranium

Mineralization

Self-heating

Biomarkers

## ABSTRACT

The effects of uranium mineralization and self-burning processes on inorganic and organic components of coal have been studied at a waste pile of the former Novátor coal and uranium mine at Bečkov (Intrasudetic Basin, Czech Republic) in order to characterize physical and chemical properties of wastes as a basis for further environmental studies. Unaltered bituminous coal was composed predominantly of vitrinite with random reflectance values between 0.72% and 0.86%, and inertinite, less common liptinite macerals, and a low level of organic solvent-extractable material (0.01–1.33 wt.%). Uranium minerals caused local radioactive alterations in the uranium-enriched coal matrix. The diameter of rounded radiation-induced haloes ranged from 0.35 to 100  $\mu\text{m}$  with higher reflectance (0.84–3.44%) compared with bulk coal. Structural changes in radiation induced altered organic coal matter were characterized by low values of Raman band disorder, fewer aliphatic C–H bonds and higher levels of oxygenated functional groups in micro-infrared spectra. Zones of higher reflectance were also confined to veinlets of epigenetic chalcopyrite, galena, and sphalerite mineralization, oriented perpendicularly to the coal bedding. The methylnaphthalene ratios (MNR) of extracted organic matter correlated with uranium concentrations in individual samples.

In self-ignition-affected samples, the higher reflectance (1.31–1.71%), and values of Raman band disorder mirrored the intensity of burning processes. Organic matter samples located at unburnt- and burnt coal interfaces were composed of a mixture of coal macerals, char and solid bitumens. In the waste heap burning zone, coal and claystone were transformed to “clinkers” composed of plagioclase, pyroxenes, tremolite, hematite, magnetite, anatase, and aluminosilicate glass or to “paralava”, formed by porous cordierite and hematite. Organic components in the burnt-out zone were represented by small dense and massive coke particles with reflectance of 4.48%, fusinite with reflectance of 3.05% and rare coke droplets of solid bitumen ( $R = 1.90\%$ ). Only traces of phenanthrene and alkanes were identified in organic extracts of burnt-out rock.

© 2016 Published by Elsevier B.V.

### 1. Introduction

The coal waste dump of the abandoned Novátor mine (at the Rybníček coal and uranium deposit, Czech Republic) was partly affected by self-burning processes. This enabled us to study and compare unaffected-(unburnt) coal and coal altered by burning processes to various degrees. Moreover, the original coal contained variable amounts of uranium, lead, copper and zinc. Therefore, aside from self-ignition processes, it was possible to study alterations in coal related to uranium and base metal mineralization.

As uranium is a common chemical element associated with coal seams, the effect of  $\alpha$ -radiation-induced coal alteration was studied by

Dill (1983), Halbach et al. (1984) and Dill et al. (1991). They concluded that radiation-induced alterations are observable by the development of anisotropic haloes surrounding accumulations of uranium minerals (coffinite, uraninite, brannerite or “uranium blacks”). Reflectance within the radiation haloes usually increases from the outer part of the halo towards the inner part, adjacent to the accumulation of uranium minerals. Smieja-Król et al. (2009) found a direct correlation between an increase in the maximum reflectance of carbonaceous materials and the concentration of uranium in the Proterozoic basin in South Africa. An increase in uranium content, from 2.5 wt.% to 15 wt.%, was accompanied by an increase in maximum reflectance from 2% to 7%, corresponding to an increase in the degree of coalification from anthracite to graphite.

The effect of radiation on organic matter (kerogen) and migrabitumens was also studied on uranium deposits in black shales, gold-uranium deposits in conglomerates, non-conforming-type

\* Corresponding author.

E-mail address: [sykorova@irms.cas.cz](mailto:sykorova@irms.cas.cz) (I. Sýkorová).

uranium or vein-type uranium deposits (Zumberge et al., 1978; Sassen, 1984; Leventhal et al., 1986; Lewan and Buchardt, 1989; Landais, 1993, 1996; Křibek et al., 1999). In summary, it was concluded that radiation damage can be responsible for an increase in the Rock Eval  $T_{max}$  and O/C values, reflectance and aromaticity values, and a decrease in H/C, and Rock Eval Hydrogen Index (HI) values of organic matter. Yields of chloroform extracts also decreased with increased radiation-induced alteration of carbonaceous matter. Micro-infrared analysis clearly shows that radiolysis effects (aliphatic C—H decrease, aromatic C—C increase) are limited to within 100  $\mu\text{m}$  of the boundary of the uraninite grains (Landais, 1996).

Very similar alterations in organic matter as in uranium deposits (i.e. increased thermal maturity, aromatization and decreased H/C ratio) were described in many types of hydrothermal Au-, Pb-, Zn-, Cu- or Hg deposits (for review, see for example Parnell et al., 1993; Glikson and Mastalerz, 2000; Greenwood et al., 2013).

It is understood that due to the negative effects of burning coal heaps on the environment (toxic fumes, subsidence, wood fires, surface and ground water contamination), much attention has been paid to solid, liquid, as well as gaseous products of coal self-burning (Finkelman, 2004; Pone et al., 2007; Stracher et al., 2011). Organic material resulting from the burning processes of coal heaps and coal seams includes altered coal matter with different reflectance, cracks, reaction rims, devolatilization pores, chars, cokes and expelled bitumens (tars), which contain many trace elements and organic compounds (Ciesielczuk et al., 2014; Emsbo-Mattingly and Stout, 2011; Misz et al., 2007; Suárez-Ruiz et al., 2012). Organics generated from carbonization cover a broad spectrum of compounds including *n*-alkanes, terpenes, simple aromatic compounds, polycyclic aromatic hydrocarbons, and phenols whose presence is dependent on the original coal material, as well as conditions during the burning processes (Emsbo-Mattingly and Stout, 2011; Misz-Kennan and Fabiańska, 2011; Misz et al., 2007; Querol et al., 2011; Ribeiro et al., 2010; Simoneit et al., 2007; Sýkorová et al., 2010). Less thermally stable compounds, such as lighter alkanes or alkylated naphthalenes and phenanthrenes are destroyed or evaporated in most self-ignition-affected materials. The emissions of aliphatic and aromatic hydrocarbons from coal fires are highly dependent on the rank of coal as well as on the conditions of thermal alteration. Low-rank and partly medium-rank coal would be expected to evolve char and tars, along with CO, CO<sub>2</sub>, hydrocarbons and gases, while higher ranked coals would have coke and less tar in the product mix (Beamish and Arisoy, 2007; Emsbo-Mattingly and Stout, 2011; Querol et al., 2011).

The present study examines the composition of mineralized coal matter in a coal waste dump, the distribution and binding of trace elements, particularly of uranium, and characterization of alterations caused by radioactive and self-burning thermal degradation. For this we have used a multi-instrumental geochemical approach, including elemental inductively coupled plasma mass spectrometry (ICP-MS), micro-petrographic (optical microscopy), scanning electron microscopy with X-ray microanalysis (ESEM/EiDX) of mineral matter, infrared and Raman spectroscopies and solvent extraction followed by gas chromatography–mass spectrometry.

The aim of present study is to contribute to our knowledge of changes that occur in the composition of mineralized coal matter during radiogenic and self-burning thermal degradation of coal waste heap materials using multi-instrumental geochemical and micro-petrographic studies. The results can be used to decipher the history of coal wastes affected by the interplay of several successive processes and to evaluate their possible environmental impacts.

## 2. Geological setting – study area

Coal and uranium were mined in the Upper Paleozoic Intra-Sudetic Basin (ISB) located at the boundary between the Czech Republic and Poland (Fig. 1). The Czech part of the ISB is filled exclusively with continental clastic and volcanoclastic deposits, mostly sub-horizontally



Fig. 1. Location of the abandoned Novátor coal and uranium mine.

bedded. Sedimentation in the basin began in the Upper Viséan and continued with some hiatuses until the Triassic (Fig. 2). The great majority of coal seams (>60) are confined to the Žacléř Formation (Westphalian A-C) or the Odolov Formation (Westphalian D to Stephanian C). Dull banded coals and banded coals sometimes with clay admixture prevail in coal seams of the ISB. Pure lithotypes as bright coals and dull coals are less abundant. In general, they belong to the category of high volatile bituminous coals with  $V^{daf}$  27–44% and vitrinite reflectance ( $R_v$ ) 0.68–1.2% (Pešek et al., 2010; Opluštil et al., 2013). The major maceral constituent was vitrinite (43–82 vol.%), while liptinite (5–27 vol.%) and inertinite (8–35 vol.%) were less abundant (Pešek et al., 2010). Less important coal seams form a part of the uppermost Stephanian and lowermost Permian formations.

Uranium mineralization in coal seams was confined to several lithostratigraphical units (Fig. 2). The Pětiletka and Lámpertice ore showings occurred in the Žacléř Formation, uranium deposits of the Kolektiv ore field in the Svatoňovice Formation, the Stachanov uranium ore field in the Radvanice Formation, and the Rybníček deposit and Chvaleč showing in the uppermost Stephanian and Autunian (Chvaleč Formation; Fig. 2).

At the former Novátor mine (the Rybníček coal and uranium deposit uranium) mineralization was composed of “uranium blacks”, coffinite and uraninite and formed small stratiform lenses from 0.1 to 0.3 m thick (Arapov et al., 1984; Bernard, 1991). Higher uranium contents were found in pyrite-rich, dull or fusinitized coal positions. Uranium was associated with elevated contents of copper (up to 1.8 wt.%), molybdenum (0.6 wt.%), lead (0.5 wt.%) and zinc (up to 0.9 wt.%). Uranium mining took place in the Rybníček deposit (the former Novátor coal and uranium mine at Bečkov) from 1952 to 1957. Roughly 300,000 tons of coal and 40,000 tons of radioactive material were extracted. Uranium contents ranged from 0.008 to 2 wt.%. Spontaneous combustion of coal heaps at the Novátor mine occurred from 1959 to 1962 (Adamec, 2015; Žáček and Skála, 2015). Since 1963 until the present time coal heaps have gradually been overgrown with vegetation, mostly birch trees.

## 3. Samples and methods

### 3.1. Samples

Samples of coal and coal claystone were taken from shallow pits, from a depth of 20–40 cm, both in unburnt and burnt parts of the heap. Additional samples were collected from a trench located at the interface between the burnt and unburnt part of the spoil heap. A total of 14 samples (approx. 0.3 kg each) were collected from all types of

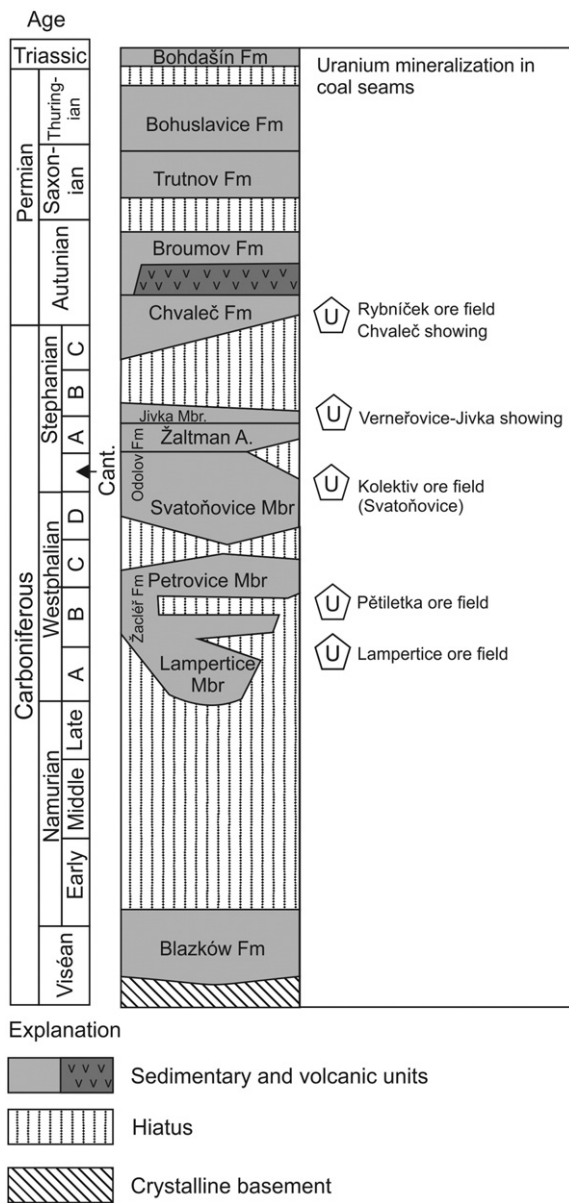


Fig. 2. Basic lithographic units in the Czech part of the Intra-Sudetic Basin with uranium ore fields or showings confined to the coal seams indicated. According to Pešek et al. (2010).

materials. In the laboratory, the samples were ground, homogenized in an agate mill to particle size  $<0.063$  mm and analyzed. Polished thin sections and polished sections were prepared for further microscopic and microprobe studies.

### 3.2. Mineralogy of coal and claystone with dispersed organic matter

Determination of the mineralogical identity of inorganic components in coal and claystone with organic admixture was attempted using a CAMECA SX 100 electron microprobe in the wavelength-dispersion mode in the Joint laboratory of Electron Microscopy and Microanalysis of the Masaryk University and Czech Geological Survey in Brno, Czech Republic. Operating conditions included an accelerating voltage of 15 kV, a beam current of 20 nA, and a beam diameter of 2  $\mu\text{m}$ , or using an electron microscope (TESCAN VEGA3XMU) equipped with an energy dispersive X-ray microanalyzer (Bruker QUANTAX200) at the Geological Institute, Czech Academy of Sciences, Prague, using

an accelerating voltage of 15 keV. The Bruker Esprit 1.9 program was used to identify the spectra.

Inorganic phase identification was carried out using a Philips X'Pert System CuK $\alpha$  diffractometer, 40 kV/40 mA, which is equipped with a secondary graphite monochromator. Records were obtained from un-oriented samples (range 3–70° 2 $\theta$ , step 0.05 2 $\theta$ /3 s).

### 3.3. Inorganic geochemistry

Concentrations of chemical elements in coal samples were established at the Bureau Veritas Mineral Laboratories Ltd. (Vancouver, Canada; former Acme Analytical Laboratories), accredited under ISO 9002 by ICP-MS. The relative percent difference (RPD) using CRM OREAS 25a and OREAS 45e standards were excellent for most chemical elements ( $\pm 10\%$  of the certified values) or good ( $\pm 10$ –25%). For Ag, Bi, Se and Sn, the RPD were higher ( $>25\%$ ) due to very low concentrations of these elements in the samples analyzed.

The amounts of carbonate carbon ( $C_{\text{carb}}$ ) organic carbon ( $C_{\text{org}}$ ) and total sulphur ( $S_{\text{tot}}$ ) were established using an ELTRA CS instrument in the accredited Central Laboratories of the Czech Geological Survey in Prague. Relative errors using reference material (CRM 7001) were  $\pm 2.5\%$  for  $\text{CO}_2$  and  $C_{\text{org}}$  and  $\pm 2\%$  for  $S_{\text{tot}}$ .

### 3.4. Organic petrology

Maceral analysis and the measurement of random reflectance of vitrinite as a rank parameter (ISO 7404-3, 2009; ISO 7404-5, 2009; ICCP, 1998, 2001) were carried out on samples from the unburnt waste zone. Reflectance values of organic matter from the burnt zone were measured as a parameter of alteration intensity (ISO 7404-3:2009, Taylor et al., 1998). Altered organic particles from burnt parts of the waste dump including: sphere, network, dense and massive textures; were evaluated according to the international classification system of thermally altered carbonaceous particles (Misz-Kennan et al., 2009 and Lester et al., 2010), which is based on principles described by (Taylor et al., 1998; Bailey et al., 1990; Vleeskens et al., 1994; Kwecińska and Petersen, 2004; Singh et al., 2007).

For petrographic analyses, polished sections were prepared and studied both in reflected and ultraviolet light using an Olympus BX51 microscope with Zeiss Photomultiplier MK3 system and fluorescence mode using an immersion lens with 40 $\times$  magnification. The Pelcon point counter was used for maceral analysis. Random and actual reflectance values were determined from particulate polished sections by SpectraVision software calibrated with sapphire ( $R = 0.596\%$ ), yttrium aluminium garnet ( $R = 0.894\%$ ), gadolinium-gallium-garnet ( $R = 1.717\%$ ), and cubic zircon ( $R = 3.12\%$ ) standards.

### 3.5. Proximate and ultimate analyses

Proximate and ultimate analyses of coal and claystones with organic admixtures were carried out using standard procedures of the International Organization for Standardisation (ISO): moisture by ISO 5069, ash by ISO 1171, and total carbon by ISO 609. The elemental organic composition was determined using a carbon, hydrogen, nitrogen, sulphur/oxygen micro-analyzer CHNS/O (Thermo Finnigan Flash FA 1112).

### 3.6. Gas chromatography/mass spectroscopy (GC/MS)

Sample extraction (cca. 20–40 g sample) and GC/MS analysis were conducted as described in detail by Havelcová et al. (2014) using the following oven temperature program: 40 °C (2 min) to 140 °C at a rate 20 °C/min, and continued at a rate 5 °C/min to 300 °C (5 min).

### 3.7. Raman spectrometry

Raman spectra of organic matter were collected from polished samples using a Thermo Scientific DXR Raman microscope equipped with a 532 nm line laser. Locations of interest were positioned using a motorized XY stage and an optical camera. The spot size of the laser focused by the 50× objective was ~1 μm in diameter. The laser power and time of sample excitation were adjusted to obtain high quality Raman spectra allowing the production of spectral maps. A laser power of 0.3 mW at the sample was used in this study. Scattered light was analyzed by a spectrograph with holographic grating (900 lines per mm) and a pin-hole width of 25 μm. The acquisition time was 10 s. Ten accumulations were added together to obtain a spectrum. A 3 μm step was selected for microspectroscopic surface mapping using the OMNIC AtPlus imaging software program (Thermo Fisher Scientific). The first-order Raman spectra of coal are dominated by two prominent features similar to those of disordered carbonaceous matter. The G band corresponds to stretching vibrations of E<sub>2g</sub> in graphitic aromatic layers. The D band was assigned to the graphite lattice mode A<sub>1g</sub> and is connected with planar defects between the basic structural units or the presence of heteroatoms (Tuinstra and Koenig, 1970). Positions, FWHM (full width at half maximum) and the intensity ratio of both bands are parameters that can describe the structure of a carbonaceous material.

### 3.8. Attenuated total reflectance - Fourier transform infrared (ATR-FTIR) spectroscopy

Infrared microspectra of the individual coal macerals were measured with a Bruker IFS 66 FTIR spectrometer combined with Hyperion IR microscope using a microATR objective equipped with a germanium crystal (diameter of 150 μm). Resulting spectra were processed with ATR correction. All spectra were recorded at a resolution of 2 cm<sup>-1</sup> with a zero-filling factor of 2. Spectra were collected from polished sections in the range of 4000–650 cm<sup>-1</sup>.

## 4. Results

### 4.1. Mineralogy of unburned and burned coal and claystone with dispersed organic matter

The mineralization of studied coal samples not affected by self-ignition consisted of: (1), grains of framboidal or euhedral pyrite, minute inclusions of galena, coffinite and uraninite scattered in coal matter (Fig. 3A,B) and, (2) base metal mineralization bound to fissures in coal matter (Fig. 3C,D,E,F). The fissures were filled with carbonates (ankerite and dolomite), quartz, kaolinite, chalcopyrite, sphalerite and galena, and probably remobilized uranium mineralization (uraninite and coffinite). In several fissures, uranium occurred in association with phosphorus, however, phosphate minerals with elevated levels of uranium were not identified.

Disseminated uraninite grains in the coal matrix or carbonate-quartz veinlets were to various degrees coffinitized (from 1.3 to 6.3 wt.% SiO<sub>2</sub>), where the coffinite contained relatively high contents of Y<sub>2</sub>O<sub>3</sub> (0.8–0.9 wt.%) and P<sub>2</sub>O<sub>5</sub> (0.8–0.9 wt.%). The anisotropic radiation-induced haloes surrounding the uraninite and coffinite grains were found in many positions in the uranium-enriched coal. Halo diameters ranged from 35 to 100 μm (Fig. 3A,B). Zones with increased reflectance also appeared along some cracks filled with kaolinite and carbonates (Fig. 3C). However, the association of these zones along mineralized fissures with uranium was not evident. Weathering of coal was manifested by the transformation of galena to cerussite, decomposition of chalcopyrite to ferric hydroxides (Fig. 3F) and malachite and by the limonitization of pyrite.

In coal and claystone samples affected by self-ignition, the composition of inorganic phases depends on the degree of thermal alteration. In less altered samples, at the interface between unburnt and burnt zones,

the original coal structures were still recognizable. However, the carbonate matrix was recrystallized, forming positions of porphyroblasts with numerous inclusions of fusinite and altered vitrinite fragments (Figs. 4A,B and 6A,B), and original aluminosilicates (clay minerals and detrital biotite and muscovite) were transformed to hydrothermal minerals such as Fe-rich chlorite or white mica (Fig. 4C). Gypsum formed scattered grains in the coal matrix. With increasing thermal alteration and dehydration, carbonates were decomposed and hydrous minerals were melted, forming “clinkers” composed of aluminosilicate glass (Fig. 4D), anhydrous aluminosilicates and silicates (pyroxenes, feldspars, Fig. 4E), titanium and ferric oxides (Fig. 4F). Wollastonite was identified by X-ray diffraction in Ca-rich coal claystone. Clinkers were accompanied by black “paralava” accumulations composed of porous cordierite and hematite.

### 4.2. Inorganic geochemistry

Unburnt samples of coal contained from 61.3 to 70.4 wt.% C<sub>org</sub>, whereas contents of C<sub>org</sub> in coal affected by self-ignition were lower (0.5 to 21.5 wt.%; Table 1). Total sulphur contents were higher in burnt samples (1.5 to 4.6 wt.% S<sub>t</sub>) than in samples not affected by self-ignition (1.3 to 2.2 wt.%). Contents of C<sub>carb</sub> in self-ignition-affected samples was generally very low (<0.05 wt.%), with the exception of samples Ry-14/1 and Ry-14/2 (2.66 and 3.08 wt.%, respectively) compared to unburnt coal samples (0.1 to 0.5 wt.%, respectively). The concentrations of trace elements were very variable in both unburnt and burnt coal samples. The highest uranium concentrations (>1000 ppm) were detected in samples Ry-4, Ry-7 and Ry-8 (Table 1). Uranium in mineralized samples was accompanied by high levels of Pb, Cu and Zn (Table 1). The concentrations of other trace elements were variable in both, unburnt and self-ignition-affected coal samples.

### 4.3. Organic petrology and extractable hydrocarbon composition of samples not affected by self-burning processes

Random reflectance values of vitrinite, from 0.72 to 0.86%, and maceral composition (Table 2) showed that samples not affected by self-burning (samples Ry-1 to Ry-8) are humic, high volatile bituminous coal with ash yields of between 12.46 and 20.42%.

The coal matter of all unburnt samples (Ry-1–Ry-8) was relatively densely interwoven with shrinkage cracks perpendicular to the stratification with a variable mineral composition (Fig. 5A) of clay minerals, sulphides, carbonates, quartz and other minerals that were described in Section 4.1.

The composition of maceral groups of vitrinite, liptinite and inertinite summarized in Table 2 showed that vitrinite macerals (48.4–71.8 vol.%), represented mainly by collotelinite and collodetrinite (Fig. 5B–F), dominated in unburnt coal samples. Other macerals of the vitrinite group, such as telinite, corpogelinite, gelinite and vitrodetrinite were less common. Their contents were below 3 vol.%. The content of pseudovitrinite in samples Ry-1 and Ry-5 was also low (below 3 vol.%), and its reflectance was up to 0.15% higher than collotelinite. The content of liptinite with weak fluorescence intensity, varied between 5.5 and 13.4 vol.%. The liptinite group macerals occurred in association with vitrinite and locally with inertinite macerals (Fig. 5C). Sporinite is the principal maceral of the liptinite group, while liptodetrinite, resinite and cutinite are less common. The inertinite macerals were the second largest component in coal samples, where contents varied between 21.4 vol.% and 41.4 vol.%. Semifusinite, fusinite, macrinite and inertodetrinite (Fig. 5A–F) were the prevailing inertinite macerals in all unburnt samples. Contents of funginite, secretinite and micrinite were below 5 vol.%.

The amounts of organic-solvent-extractable compounds in unburnt samples were generally low (0.02–1.33 wt.%), and, according to results of GC/MS analyses, the samples can be classified into two types:

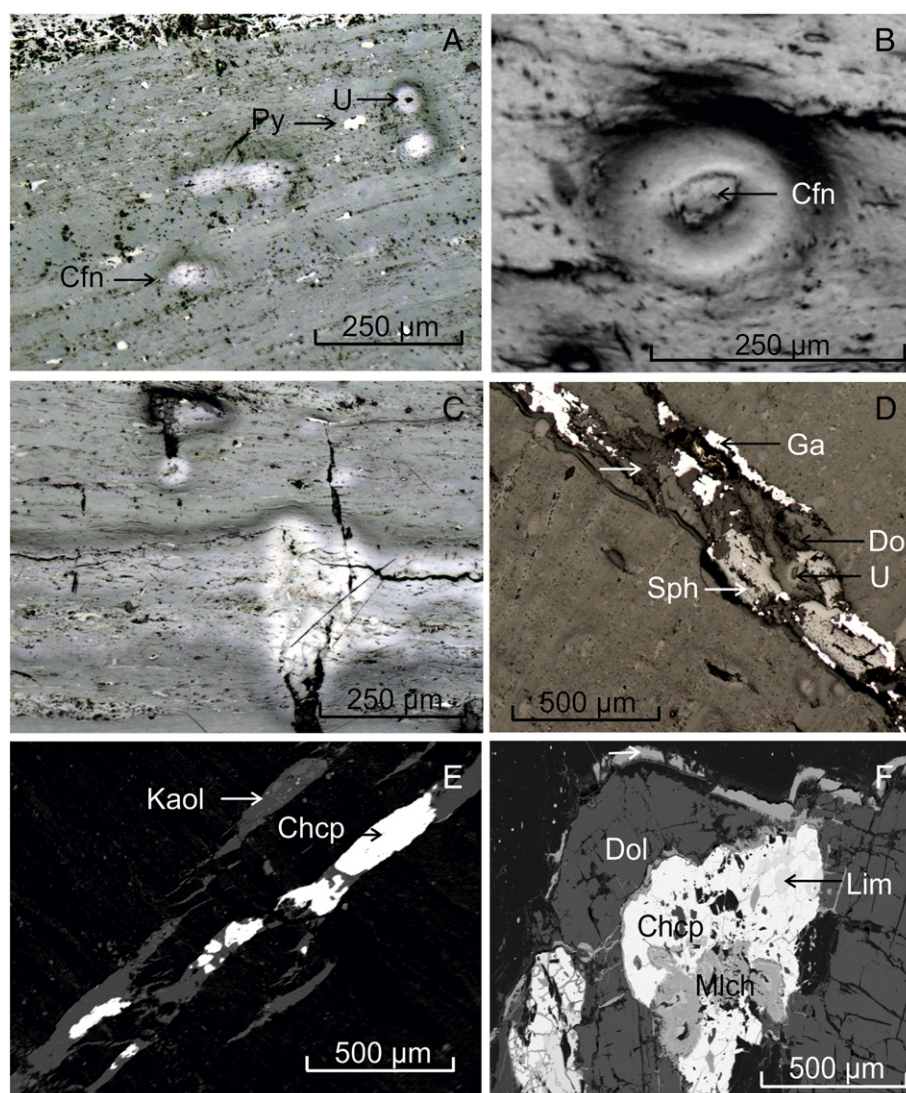


**Fig. 3.** Photomicrographs (A, B, C, D) and BSE images (E, F) of mineralized coal from the Rybníček deposit (Novátor mine). A: Stratiform uranium and sulphide mineralization in the coal seam. Mineralization consists of disseminated grains of euhedral or framboidal pyrite, uraninite and coffinite. Sample Ry-4. B: Close-up of the radiation-induced halo surrounding the grain of coffinite. Stratiform types of mineralization. Sample Ry-4. C: Zones of high reflectance form a rim of the epigenetic sulphide and remobilized uranium mineralization. Cracks and fissures are partly filled in with carbonates (dark grey). An association of these high reflectance zones with uranium mineralization was not found. Sample Ry-7. D: Galena-sphalerite-carbonate mineralization with minute grain of uraninite confined in fissures of coal. Sample Ry-2. E: Fissure in coal healed by kaolinite (dickite?) and chalcopyrite. Sample Ry-2. F: A part of a dolomite veinlet with chalcopyrite affected by weathering processes. Chalcopyrite is partly decomposed to a mixture of chalcopyrite and limonite or replaced by malachite. Sample Ry-2. *Explanation of symbols:* Py = pyrite, U = uraninite, Cfn = coffinite, Dol = dolomite, Kaol = kaolinite, Ga = galena, Sph = sphalerite, Chcp = chalcopyrite, Lim = limonite, Mlch = malachite.

**Type 1 (samples Ry-1–Ry-5):** The sample extracts had *n*-alkane distributions in the range from *n*-C<sub>11</sub> to *n*-C<sub>27</sub>, and the distribution was either uniform (Fig. 6A) or of mixed type with lower *n*-alkanes dominating (Fig. 6B) or middle *n*-alkanes dominating (Fig. 6C) and with different maxima (Table 3). Carbon preference indices (CPI<sub>24–34</sub>; Table 3), reflecting the odd-over-even carbon atom number predominance for *n*-C<sub>24</sub>–*n*-C<sub>34</sub> alkanes, were low. The acyclic isoprenoids pristane (Pr) and phytane (Ph) were identified, as well as the sesquiterpenes: eudalene and cadalene. The extracts contained high concentrations of aromatic compounds, comprising unsubstituted PAHs with 2–4 aromatic rings in a molecule: naphthalene, phenanthrene, and fluoranthene, together with substituted naphthalenes, phenanthrenes, and dibenzofurans. C<sub>1</sub>–C<sub>4</sub> alkyl naphthalenes (up to about 40%) were dominant in the PAH group (Fig. 7A) together with C<sub>1</sub>–C<sub>3</sub> alkyl phenanthrenes (Fig. 7B) (up to about 15%) whereas methylpyrenes were only detected at low concentrations (up to about 2%). To assess the variance of alkyl aromatic hydrocarbon

distributions between the samples, the methyl naphthalene ratio was calculated. Limited concentrations of the other compounds make them unreliable as parameters for other ratios and indices used in geochemistry. Other PAHs were not present, except pyrene at a low concentration. The aromaticity of the sample extracts, i.e. the proportion of aromatic compounds to all identified compounds, was very high (63–88%), and unsubstituted PAHs comprised 13–28%. **Type 2 (samples Ry-7 and Ry-8):** *n*-Alkanes ranged from *n*-C<sub>14</sub> to *n*-C<sub>28</sub>. Middle-chain *n*-alkanes predominated in the spectra (Fig. 6C; Table 3). The extracts showed a slight predominance of odd-over-even carbon atom number *n*-alkanes and CPI values were lower than the Type 1 samples. Pristane, phytane and terpenes were not identified. Extracts of this type of sample also contained high concentrations of lighter aromatic compounds (naphthalene, phenanthrene, and fluoranthene), together with substituted naphthalenes, and phenanthrenes (including phenanthrol), but the distribution was different compared with the Type 1 samples (Fig. 7). The

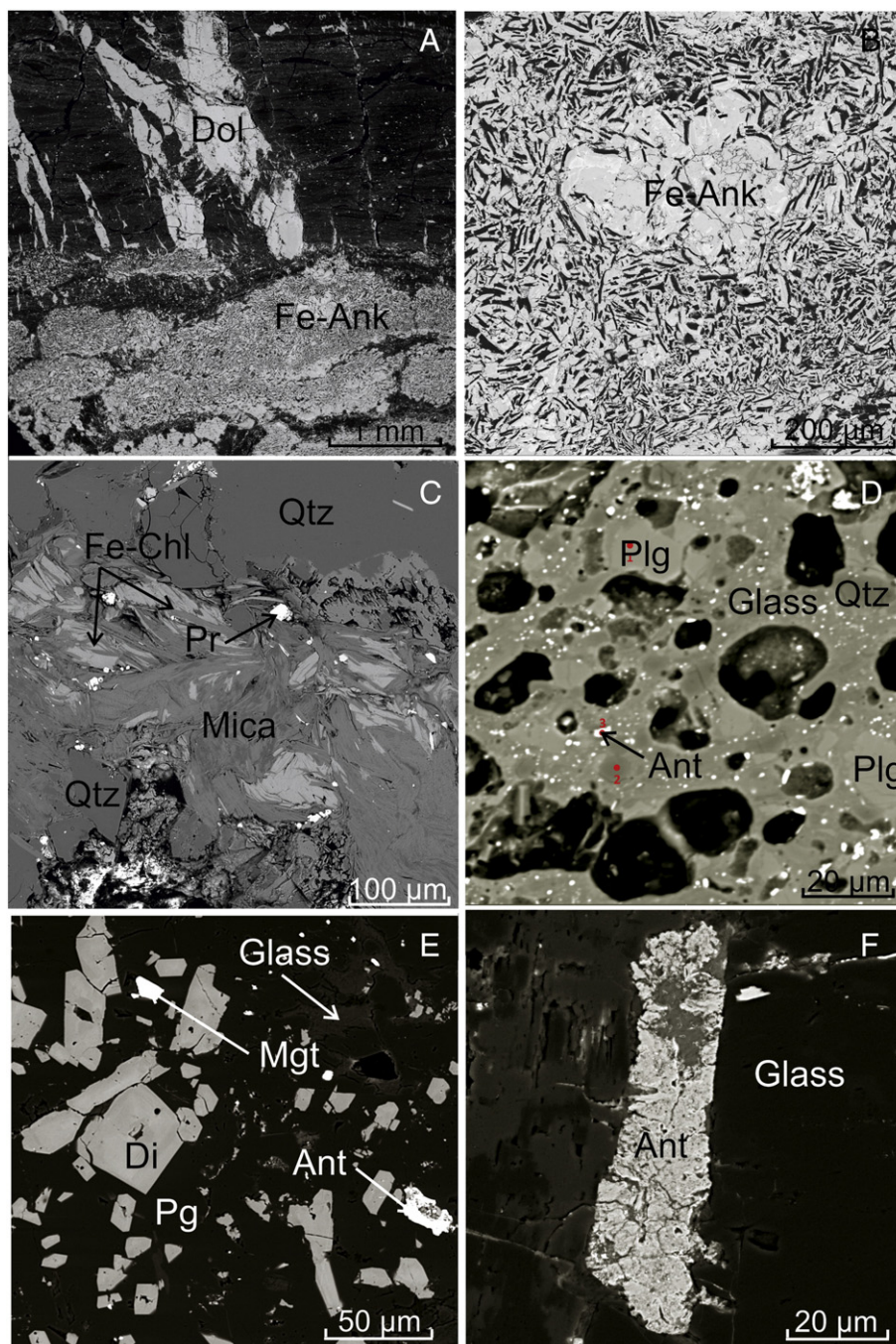


**Fig. 4.** BSE images of coal samples and claystones affected by self-ignition. A, B: Low-grade (hydrous) alteration of coal. Veinlets of older hydrothermal dolomite in the coal matrix are overprinted by porphyroblasts of Fe-ankerite with numerous black fragments of fusinite. Sample Ry-14/2. B: Close-up of previous image. C: Low-temperature (hydrous) alteration of coal claystone is indicated by the development of Fe-chlorite and white mica flakes in plagioclase and quartz-rich matter. Sample Ry-14/1. D: High-temperature (anhydrous) alteration of coal claystone. The matrix is composed of aluminosilicate glass with plagioclase and remnants of quartz grains. Sample voids, in some places, filled with bitumen. Sample Ry-9. E: High-temperature alteration of claystone. Sample is composed of diopside, anorthite and aluminosilicate glass with disseminated particles of anatase. Sample Ry-9. F: High-temperature alteration. Anatase grain embedded in aluminosilicate glass. Sample Ry-9. *Explanation to abbreviations:* Ant = anatase, Di = pyroxene (diopside), Dol = dolomite, Fe-Ank = ankerite, Fe-Chl = chlorite, Glass = aluminosilicate glass, Mgt = magnetite, Mica = Na–K-white mica, Pg = plagioclase, Pr = pyrrhotite, Qtz = quartz.

aromaticity of Ry-7 and Ry-8 sample extracts was high (84 and 69%), unsubstituted PAHs comprised 6–8%, and extractable compound yields of this sample type were lower (Table 3).

#### 4.4. Radiation induced alteration of unburned samples

Radiation-induced alterations to organic matter were studied in samples with high uranium content (>100 ppm U; samples Ry-4, Ry-7

and Ry-8; Table 1). The average reflectance of haloes ( $\bar{\theta}_{RA}$ ), the number of measured objects (n), and the radiation-induced total organic matter (RA-OM) content, including altered vitrinite and liptinite, are listed in Table 2. The occurrence of bright zones with “haloes” was associated with vitrinite-rich detrital layers (Fig. 5C), where collodetrinite with disseminated fragments of inertinite and liptinite macerals prevailed over collotelinite and semifusinite (Fig. 5C–F). The radiation-induced haloes particularly surrounding grains of coiffinite, were rare in sample Ry-2, but were found in many positions in samples Ry-4–

Table 1

Geochemical composition of unburnt and burnt coal and claystone.

| Sample/component  | Ry-1         | Ry-2   | Ry-3  | Ry-4     | Ry-5  | Ry-7   | Ry-8     | Ry-9                     | Ry-13/1 | Ry-13/2 | Ry-14/1 | Ry-14/2 |
|-------------------|--------------|--------|-------|----------|-------|--------|----------|--------------------------|---------|---------|---------|---------|
|                   | Unburnt coal |        |       |          |       |        |          | Burnt coal and claystone |         |         |         |         |
| <i>(wt.%)</i>     |              |        |       |          |       |        |          |                          |         |         |         |         |
| Al                | 0.73         | 1.38   | 1.56  | 0.85     | 1.14  | 0.94   | 0.77     | 0.69                     | 5.71    | 4.56    | 5.42    | 5.93    |
| Fe                | 0.86         | 1.96   | 1.81  | 0.58     | 0.58  | 0.57   | 0.50     | 6.82                     | 5.34    | 2       | 3.88    | 3.30    |
| Ti                | 0.032        | 0.060  | 0.080 | 0.043    | 0.060 | 0.049  | 0.041    | 0.02                     | 0.26    | 0.22    | 0.26    | 0.28    |
| Ca                | 0.64         | 0.29   | 1.18  | 0.89     | 1.41  | 0.75   | 0.78     | 6.90                     | 0.32    | 0.56    | 1.34    | 1.62    |
| Mg                | 0.21         | 0.16   | 0.67  | 0.18     | 0.43  | 0.15   | 0.13     | 2.17                     | 0.48    | 0.32    | 0.65    | 0.68    |
| K                 | 0.14         | 0.19   | 0.44  | 0.14     | 0.22  | 0.18   | 0.15     | 0.09                     | 2.37    | 1.68    | 1.96    | 2.02    |
| P                 | 0.148        | 0.133  | 0.144 | 0.287    | 0.238 | 0.257  | 0.290    | 0.20                     | 0.18    | 0.09    | 0.17    | 0.21    |
| S <sub>tot</sub>  | 1.27         | 2.24   | 1.78  | 2.12     | 1.04  | 2.01   | 1.78     | 4.58                     | 1.85    | 1.47    | 1.49    | 1.68    |
| C <sub>org</sub>  | 69.63        | 66.68  | 61.27 | 69.24    | 66.61 | 67.62  | 70.41    | 0.51                     | 1.24    | 1.47    | 21.53   | 20.88   |
| H                 | 4.02         | 3.77   | 3.39  | 3.99     | 3.88  | 3.99   | 4.18     | 0.07                     | 0.13    | 0.12    | 1.32    | 0.50    |
| N                 | 3.54         | 2.90   | 3.13  | 2.34     | 2.64  | 1.18   | 1.06     | 0.01                     | 0.02    | 0.02    | 1.54    | 0.47    |
| CO <sub>2</sub>   | 0.68         | 0.19   | 1.62  | 0.46     | 1.65  | 0.39   | 0.35     | <0.05                    | <0.05   | <0.05   | 8.76    | 10.13   |
| C <sub>carb</sub> | 0.21         | 0.06   | 0.49  | 0.14     | 0.50  | 0.12   | 0.11     | <0.05                    | <0.05   | <0.05   | 2.66    | 3.08    |
| <i>(ppm)</i>      |              |        |       |          |       |        |          |                          |         |         |         |         |
| Ag                | 4.0          | 11.0   | 8.4   | 12.6     | 0.9   | 7.6    | 6.8      | 5.5                      | 4.4     | 2.9     | 5.3     | 4.4     |
| As                | 66           | 99     | 72    | 73       | 7     | 61     | 54       | 186                      | 281     | 39      | 181     | 168     |
| Bi                | 0.4          | 0.9    | 1.1   | 0.4      | 0.4   | 0.5    | 0.4      | 0.1                      | 4.5     | 2.3     | 2.1     | 2.8     |
| Cd                | 3.8          | 2.6    | 2.9   | 113.4    | 8.7   | 82.9   | 61.4     | 50.5                     | 10      | 24.4    | 31.7    | 28.4    |
| Co                | 4.8          | 14.2   | 18.2  | 8.1      | 1.8   | 4.1    | 5.4      | 28.1                     | 5.1     | 2.8     | 23.1    | 24.3    |
| Cr                | 5            | 11     | 15    | 8        | 8     | 8      | 8        | 36                       | 82      | 105     | 92      | 95      |
| Cu                | 1332         | 9410   | 8609  | 406      | 2952  | 758    | 336      | 337                      | 631     | 1249    | 4405    | 3262    |
| Hg                | 0.20         | 0.28   | 0.37  | 0.58     | 0.48  | 0.57   | 0.52     | 0.47                     | 6.57    | 43.44   | 0.27    | 0.58    |
| Mn                | 199          | 61     | 615   | 93       | 339   | 75     | 68       | 1956                     | 75      | 39      | 117     | 143     |
| Mo                | 16           | 75     | 39    | 444      | 10    | 260    | 254      | 91                       | 30      | 20      | 52      | 62      |
| Pb                | 2043.6       | 2211.2 | 321.7 | 19,574.0 | 305.5 | 4244.0 | 15,740.0 | 9581.1                   | 6450.1  | 3708    | 7582.2  | 3525.7  |
| Sb                | 12           | 21     | 15    | 30       | 8     | 17     | 15       | 38                       | 15      | 11      | 10      | 9       |
| Se                | 2            | 3      | 2     | <1       | 1     | <1     | 2        | 7                        | 103     | 65      | 44      | 47      |
| Sn                | 0.4          | 2.6    | 1.3   | 0.6      | 0.9   | 0.8    | 0.6      | 0.5                      | 8       | 5.4     | 6.1     | 6.3     |
| Th                | 3            | 5      | 6     | 3        | 5     | 4      | 3        | 1                        | 24      | 14      | 14      | 15      |
| U                 | 42           | 153    | 36    | 1176     | 569   | 1115   | 1287     | 100                      | 60      | 69      | 551     | 273     |
| Y                 | 27           | 54     | 37    | 64       | 52    | 41     | 83       | 47                       | 18      | 34      | 57      | 45      |
| Zn                | 375          | 318    | 270   | 9621     | 521   | 6495   | 5405     | 4355                     | 668     | 1410    | 1054    | 1497    |
| Zr                | 12           | 305    | 12    | 3        | 4     | 7      | 2        | 34                       | 99      | 96      | 112     | 123     |

S<sub>tot</sub> – total sulphur content (dry basis); C<sub>org</sub> – organic carbon content (dry basis); C<sub>carb</sub> – carbonate carbon content (dry basis); H – hydrogen content (dry basis); N – nitrogen content (dry basis).

Ry-8. The halo volumes ranged from 4 vol.% in sample Ry-5 up to 14.6 vol.% in sample Ry-8. Due to the radiation-induced alteration, the average reflectance of vitrinite increased from 1.52% (Ry-4) to 1.75% in sample Ry-8, in the bright zones (Table 2). Detailed reflectance measurements in different parts of haloes found two types of light zones around the grains of uranium minerals. The first type is dominant and represents a halo with minimal relief and reflectance increasing from 0.70% on the edge of the halo to a maximal reflectance value of 1.62% in contact with the grain of uranium mineral (Fig. 5D). The second type is represented by the halo in Fig. 5E. These haloes are characterized by a strong relief and a rapid increase in reflectance from 0.74% in a dark rim to a maximal reflectance value higher than 3% (3.44%) in the lightest part in contact with the grain of uranium mineral.

Compared to vitrinite the reflectance of liptinite macerals increased from 0.30% to 0.90% (Fig. 5D) and the fluorescent colour of liptinite changed from yellow through orange to reddish brown. Bright zones with maximal values of reflectance up to 1.65% also appeared along fissures (Fig. 5F).

Representative Raman spectra of radiation unaffected vitrinite and inertinite macerals and radiation-affected coal are shown in Fig. 8. In the spectral region of 900 and 1800 cm<sup>-1</sup>, the D and G bands of carbonaceous matter were curve-fitted using Lorentzian function, and FWHM of the D band was used as a parameter proportional to the degree of radiation-induced alteration of coal. The average parameters of G and D bands and their intervals for radiation unaffected and affected coal are shown in Table 4. Fig. 9 shows a good correlation between the average D bandwidth (FWHM) and the average reflectance of vitrinite of unburnt coal, haloes in samples Ry-4 to Ry-8 and carbonaceous matter of self-ignition-affected samples Ry-9, Ry-13 and Ry-14 measured at the

polished section. In order to assess changes in D bandwidth data across the radiation-induced halo, a suitable rectangle halo area with dimensions 126 × 93 μm (mapping step 3 μm) was chosen for Raman micro-spectroscopy mapping (see Fig. 10A). The map of this area based on Raman spectral features in the range 1800–900 cm<sup>-1</sup>, is shown in Fig. 10B. The map shows that the halo surface is not homogenous. The blue spot (crack) in the middle of the halo is a grain of coffinite. In Fig. 10C, the D bandwidth value profile across the halo is illustrated. The results indicate that the average value of the FWHM D gradually decreased from ~310 to ~220 cm<sup>-1</sup>, from the halo periphery to the halo central part.

Using ATR-FTIR micro-spectroscopy, structural differences between the halo and its surroundings were studied. The infrared spectra of the radiation-induced halo, and its surroundings, are shown in Fig. 11, together with a difference spectrum obtained by subtracting the surrounding spectrum from the spectrum of the halo. From the different spectral features it is obvious that the organic structure of the halo contains a smaller content of aliphatic C–H bonds (negative bands at 2927, 2855, 1447 cm<sup>-1</sup>) and higher content of oxygenated functional groups (positive features at 3432, 1747, 1686, 1400, 1332, 1238, 1043 cm<sup>-1</sup>).

From these spectral features, it can be deduced that strong alterations in the halo take place due to radiolytic cleavage of aliphatic structures to form esters (1747 cm<sup>-1</sup>), carboxylic acids (1689 cm<sup>-1</sup>) and alkanols (3434 cm<sup>-1</sup>). In addition, one positive band at 876 cm<sup>-1</sup> and two negative bands at 817 and 754 cm<sup>-1</sup> were found in the difference IR spectrum. These bands can be assigned to the out-of-plane vibrations of C–H bonds of isolated, two and four adjacent hydrogens in an aromatic-substituted system (Ibarra et al., 1996). The number of adjacent hydrogens per ring provides an estimation of the degree of

**Table 2**  
Ash yield, random and average reflectance values (%) and petrographic composition (vol.% mmf) of unburnt and burnt coal and claystone.

| Sample/parameter   | Ry-1  | Ry-2  | Ry-3  | Ry-4  | Ry-5  | Ry-7  | Ry-8  | Ry-9  | Ry-13/1 | Ry-13/2 | Ry-14/1 | Ry-14/2 |
|--|-------|-------|-------|-------|-------|-------|-------|-------|---------|---------|---------|---------|
| A <sup>d</sup> (%)   | 14.48 | 16.74 | 20.42 | 13.19 | 17.81 | 15.79 | 12.46 | 98.71 | 97.80   | 97.69   | 42.46   | 56.45   |
| R <sub>r</sub> (%)   | 0.72  | 0.77  | 0.86  | 0.74  | 0.73  | 0.79  | 0.80  | –     | –       | –       | –       | –       |
| σ  | 0.04  | 0.08  | 0.10  | 0.09  | 0.07  | 0.08  | 0.09  | –     | –       | –       | –       | –       |
| ∅ R <sub>RAV</sub> (%)   | –     | 0.94  | 0.0   | 1.52  | 1.60  | 1.63  | 1.75  | –     | –       | –       | –       | –       |
| <i>n</i>   | –     | 5     | –     | 41    | 17    | 50    | 75    | –     | –       | –       | –       | –       |
| ∅ R <sub>TAV</sub> (%)   | –     | –     | 0.96  | –     | –     | –     | –     | –     | –       | –       | 1.77    | 1.31    |
| <i>n</i>   | –     | –     | 10    | –     | –     | –     | –     | –     | –       | –       | 60      | 75      |
| ∅ R <sub>BOM</sub> (%)   | –     | –     | –     | –     | –     | –     | –     | 3.42  | 2.84    | 3.65    | 2.13    | 2.05    |
| <i>n</i>   | –     | –     | –     | –     | –     | –     | –     | 40    | 45      | 50      | 200     | 200     |
| R <sub>Fus</sub> (%)   | –     | –     | –     | –     | –     | –     | –     | –     | –       | –       | 2.04    | 2.65    |
| R <sub>Coke</sub> (%)  | –     | –     | –     | –     | –     | –     | –     | 4.48  | 3.59    | 4.52    | 2.13    | 2.26    |
| R <sub>Bit</sub> (%)   | –     | –     | –     | –     | –     | –     | –     | 2.74  | 0       | 2.77    | 1.80    | 2.13    |
| <i>Forms of organic matter (vol.% mmfb)</i>                                  |       |       |       |       |       |       |       |       |         |         |         |         |
| Unburnt OM   | 100.0 | 99.0  | 95.7  | 90.9  | 94.1  | 90.0  | 85.4  | –     | –       | –       | –       | –       |
| Rad. Alter. OM   | –     | 1.0   | –     | 9.1   | 3.4   | 10.0  | 14.6  | –     | –       | –       | –       | –       |
| Therm. Alter. OM   | –     | –     | 4.3   | –     | –     | –     | –     | –     | –       | –       | 89.1    | 90.9    |
| Burnt OM   | –     | –     | –     | –     | –     | –     | –     | 100.0 | 100.0   | 100.0   | 10.9    | 9.1     |
| <i>Composition of maceral groups and altered organic matter (vol.% mmfb)</i> |       |       |       |       |       |       |       |       |         |         |         |         |
| ∑ VITRINITE  | 56.6  | 71.8  | 55.0  | 53.1  | 68.4  | 53.2  | 48.4  | 7.1   | –       | –       | 35.1    | 56.1    |
| Vitrinite <sub>UBV</sub>   | 53.8  | 68.4  | 47.8  | 42.5  | 62.1  | 40.9  | 31.5  | –     | –       | –       | –       | –       |
| Pseudovitrinite  | 2.8   | 2.3   | 2.9   | 2.4   | 2.9   | 2.5   | 2.6   | –     | –       | –       | –       | –       |
| Vitrinite <sub>RA</sub>  | 0.0   | 1.1   | 0.0   | 8.2   | 3.4   | 9.8   | 14.3  | –     | –       | –       | –       | –       |
| Vitrinite <sub>TA</sub>  | 0.0   | 0.0   | 4.3   | –     | –     | –     | –     | 7.1   | –       | –       | 35.1    | 56.1    |
| ∑ LIPTINITE  | 9.9   | 6.8   | 13.4  | 5.5   | 9.3   | 12.4  | 9.8   | –     | –       | –       | 2.2     | 1.2     |
| Liptinite <sub>UBV</sub>   | 9.9   | 6.8   | 12.6  | 4.6   | 8.7   | 9.2   | 9.5   | –     | –       | –       | –       | –       |
| Liptinite <sub>RA</sub>  | –     | –     | –     | 0.9   | 0.6   | 0.2   | 0.3   | –     | –       | –       | –       | –       |
| Liptinite <sub>TA</sub>  | –     | –     | 0.8   | –     | –     | –     | –     | –     | –       | –       | 2.2     | 1.2     |
| ∑ INERTINITE   | 35.3  | 21.4  | 31.6  | 41.4  | 22.3  | 33.4  | 31.8  | 9.3   | 0.0     | 0.0     | 51.8    | 33.6    |
| FUSINITE   | –     | –     | –     | –     | –     | –     | –     | –     | –       | –       | 29.1    | 15.2    |
| COKE   | –     | –     | –     | –     | –     | –     | –     | 77.2  | 100.0   | 100.0   | 9.1     | 5.2     |
| Network  | –     | –     | –     | –     | –     | –     | –     | 17.3  | 15.6    | 12.4    | 1.0     | 1.7     |
| Dense  | –     | –     | –     | –     | –     | –     | –     | 10.3  | 9.6     | 7.5     | 4.6     | 2.3     |
| Massive  | –     | –     | –     | –     | –     | –     | –     | 22.8  | 24.9    | 29.3    | 0.9     | 1.2     |
| Fragments  | –     | –     | –     | –     | –     | –     | –     | 20.4  | 49.9    | 43.8    | 2.6     | –       |
| BITUMEN  | –     | –     | –     | –     | –     | –     | –     | 6.4   | 0.0     | 7.0     | 1.8     | 3.9     |

A<sup>d</sup> – ash yield (d – dry basis), R<sub>r</sub> = random reflectance, rank parameter (%), σ = standard deviation, ∅ R<sub>RAV</sub> = average reflectance of haloes and bright zones around fissures; ∅ R<sub>BOM</sub> = average reflectance of burnt organic matter, coke and bitumen; R<sub>Fus</sub> = average reflectance of fusinite in carbonates; R<sub>Coke</sub> = average reflectance of coke walls; R<sub>Bit</sub> = average reflectance of bitumens; mmfb – mineral matter free basis. The number of measured points is in italic.

aromatic substitution and condensation with increasing alteration within radiation-induced haloes.

#### 4.5. Self-ignition affected samples

Self-ignition-affected samples were of two types: Samples Ry-14/1–2 were collected at the interface of unburnt and burnt zones of a waste pile and represent coaly claystone with organic carbon contents of 21.53% and 20.88% respectively, and a total sulphur content of about 1.50%. Samples (Ry-9 and Ry-13/1–2) represented burnt-out rocks (“clinkers”) with dispersed organic matter (0.51–1.47%), with a total sulphur content of 1.47% to 4.58% (Table 1).

Samples Ry-14/1 and Ry-14/2 were composed of a mixture of clasts of altered coal matter, coke and solid bitumen (Table 2) cemented by carbonates, quartz and hydrous aluminosilicates (white mica and chlorite). Results in Table 2 show that clasts of altered coal matter dominated with distinguishable macerals of vitrinite and inertinite, particularly fusinite (Fig. 12A and B). Clasts of altered coal were formed by collotelinite and collodetrinite with numerous cracks, fine pores and higher reflectance values of 1.31% and 1.77%, a smaller portion of inertinite containing anisotropic semifusinite, and rare liptinite with reflectances up to 0.90% (Fig. 12B). The significance for these samples was the occurrence of clasts of fusinite, impregnated with carbonates and quartz, with reflectance about 3.05% (Table 2; Fig. 4B and 12A,B). Coke particles, with a dense and crassi-network texture (Fig. 12C,D), and average reflectance values of about 2.25%, sometimes with weak mosaic and inertinite optical anisotropy, were also cemented by carbonates and clay minerals. Particles of solid bitumen with irregular shapes, strong relief and reflectance values up to 2.13% (Fig. 12E) were rare.

The fine-grained burnt claystone (clinker) Ry-9 only contained small amounts of minute carbonaceous particles with average reflectance values of 3.42%, which were disseminated in the walls of a porous mineral matrix (Fig. 11F). Fusinite, dense and massive coke particles (Fig. 11G) and droplets of solid bitumen (R = 1.90%) predominated in this sample while particles of altered and brecciated coal matter, including vitrinite, macrinite and liptinite were rare (Fig. 11H). A similar, thermally altered claystone forms the basis of samples Ry-13/1 and Ry-13/2 with reflectance values ranging from 1.48% to 4.74%.

Because of the small size and high thermal degradation of carbonaceous particles, it was not possible to record their infrared spectra. Therefore, structural changes of organic matter of burnt materials were studied by Raman spectrometry only. Fig. 9 shows the smallest values of the average D bandwidth (FWHM at 179 and 156 cm<sup>-1</sup>) which corresponded with the highest average reflectance values, and therefore a higher degree of thermal degradation. On the other hand both parameters of samples Ry-14/1 and Ry-14/2 corresponded with lower degrees of thermal alteration.

Compared to unburnt samples, the yields of extractable compound from samples affected by self-burning were very low (0.01–0.04 wt.%) and extracts were very poor in identifiable organic compounds. Compounds detected in burnt samples were phenanthrene, and benzotriazole, with phthalates as a contaminant. Only in an extract of sample Ry-9 were traces of *n*-alkanes identified, having chain carbon numbers from *n*-C<sub>18</sub> to *n*-C<sub>27</sub>. In spite of the application of activated copper, chromatographic results were affected by the presence of elemental sulphur (mainly Ry-13/1 and Ry-13/2).

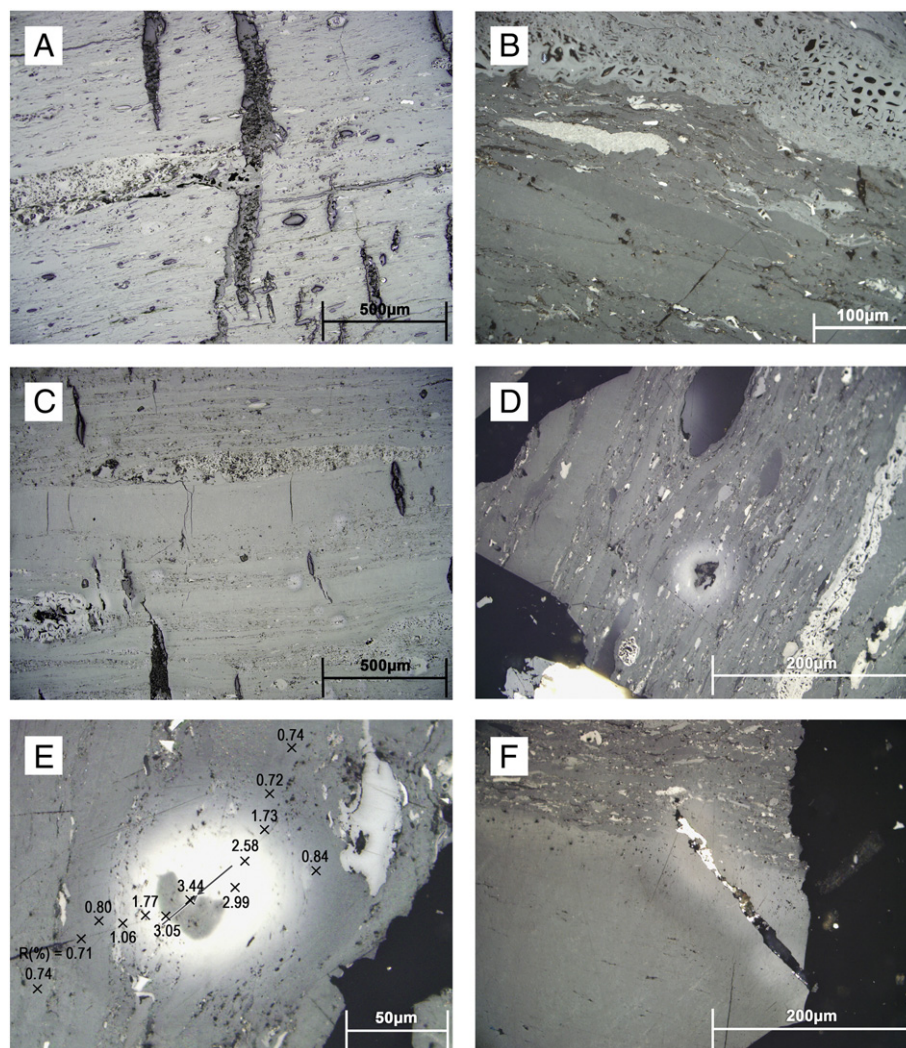


**Fig. 5.** Photomicrographs of organic matter from unburnt coal waste zone of the Rybníček deposit. A: Vitritine of sample Ry-1 with disseminated fine grains of liptinite, inertinite macerals, grains of quartz. Light semifusinite band in the central part of photomicrograph is broken by mineralized fissures perpendicular to the stratification. B: Collotelinite band between collodetrinite layers with dispersed sporinite, liptodetrinite, inertodetrinite, semifusinite and macrinite, and semifusinite at the top of the image. Sample Ry-2. C: Stratiform uranium mineralization in coal matter. Bright zones of high reflectance around the grains in haloes dispersed in collodetrinite and around some cracks. The central collotelinite band shows broken shrinkage cracks. Sample Ry-4. D: Coal matter formed by a collotelinite band and collodetrinite layers with dispersed small fragments of liptinite and inertinite macerals with dark grey fragments of sporinite and a light band of semifusinite. Close-up of the moderate radiation-induced halo with reflectance of vitritine increases from 0.73% to 1.62% in contact with the grain of coiffinite in collodetrinite. The zone with higher reflectance occurred in sporinite. Sample Ry-7. E: High reflectance halo with marked vitritine reflectance values, which increase from the dark edge to the contact with a uraniferous phase. Sample Ry-8. F: Zones of high reflectance form a rim of epigenetic sulphide and probable remobilized uranium mineralization in collotelinite and partly in collodetrinite. Sample Ry-7. Photomicrographs B, D, E, F were taken in reflected white light using an immersion lens with 40 $\times$  magnification and photomicrographs A and C using a dry lens with 20 $\times$  magnification.

## 5. Discussion

### 5.1. Coal mineralization

Coal from the Novátor mine was, to a variable degree, mineralized. Results of principal component analyses revealed that 73.4% of the dispersed variables could be assigned to two factors (eigenvalue >1; Fig. 13). High values of Factor 1 characterize Al, Ti, Zr, Th, Rb and K, i.e., elements confined to aluminosilicates, titanium oxides and minerals of zirconium.

In contrast, negative Factor 1 values are characteristic of  $C_{org}$ , P, U and Hg. Therefore, Factor 1 can be interpreted in terms of the inorganic to organic matter ratio in the samples studied. High positive Factor 2 loadings for Ca,  $C_{carb}$ , Mg and Mn values and low (close to -1) Factor 2 loadings for  $S_{tot}$ , Ag, As and Sb indicate that Factor 2 can be interpreted as the carbonate-to-sulphur ratio in coal samples.

Many other chalcophilic elements display negative Factor 2 values, indicating an association with sulphur. However, they may be

subdivided into two groups: (1) Cd, Zn, Pb, Mo and Y project close to  $C_{org}$ , whereas (2) Bi, Co, Cu, Cr, Se and Sn group with Fe. Therefore, the results of principal component analysis revealed that two types of mineralization were present in the samples:

- (1) Stratabound, syngenetic uranium mineralization (association of P, U, Hg, Y, Cd, Zn, Pb and Mo) with organic matter ( $C_{org}$ ) and,
  - (2) Epigenetic, base metal mineralization ( $S_{tot}$ , Ag, As, Bi, Co, Cu, Cr, Fe, Se, Sb, Sn) confined to small veinlets perpendicular to or oblique to the coal bedding. A close association of Cu and other elements with Fe reflects the occurrence of chalcopyrite.
- (1) The association of uranium with organic matter has been described many times in the literature. Uranium in the +6 (oxidized) state can be readily fixed by organic material in a process that does not require an immediate reduction of uranium (Szalay, 1964; Schmidt-Collerus, 1969; Jennings and Leventhal, 1977; Křibek and Podlaha, 1980). Reduction from the +6 to +4 state and the formation of uranium mineralization

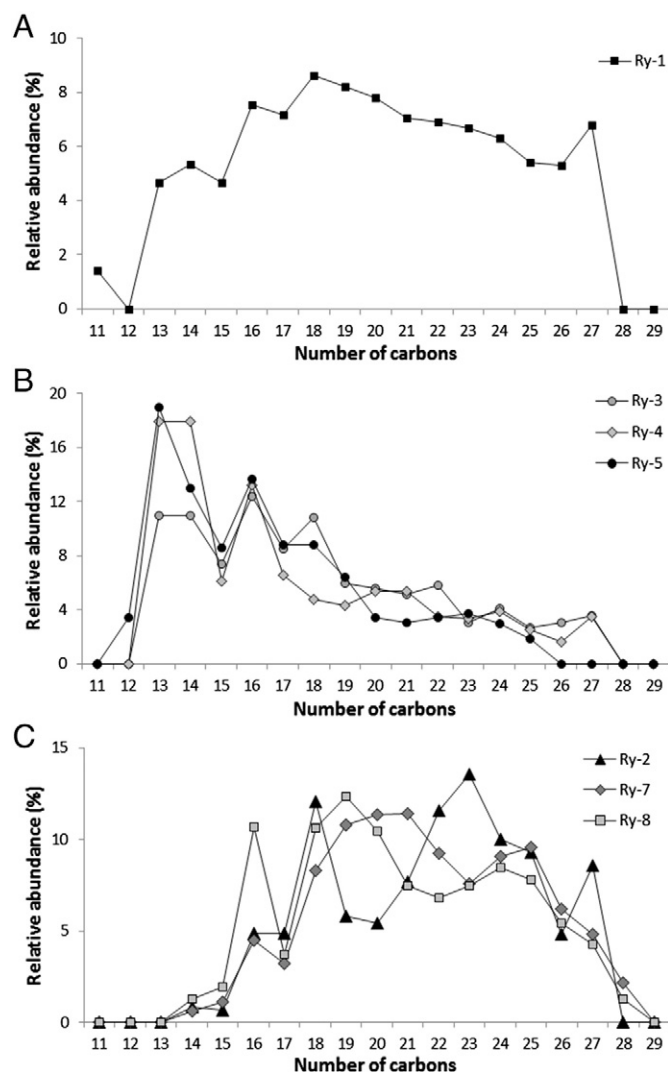


Fig. 6. The distribution of *n*-alkanes in A) Type 1 samples (Ry-1 and Ry-2), B) Type I samples (Ry-3–Ry-5) and C) Type 2 samples (Ry-7 and Ry-8). (SIM 85 m/z).

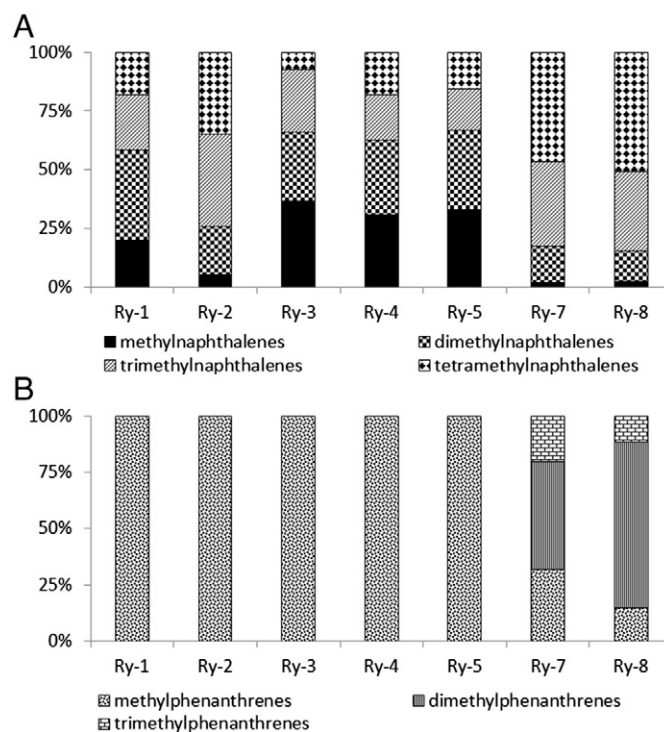


Fig. 7. The distribution of A) naphthalenes and B) phenanthrenes in samples. (SIM 142 + 156 + 170 + 184 m/z, and 192 + 206 + 220 m/z).

can occur at some later time due to the decrease in carboxyl and carbonyl functions during coalification (Kochenov et al., 1977). The ubiquitous association of coffinite or uraninite with organic matter and the occurrence of inclusions of organic matter in many sedimentary coffinites imply that the presence of amorphous organic matter as a strong sorbent and reductant (or as a substrate for biogenic H<sub>2</sub>S) may be critical to coffinite and uraninite formation at temperatures <200 °C (Fuchs and Hoekstra, 1959; Smith, 1984). The black colour, characteristic of coffinite in coal, may be due to an admixture of organic carbon. X-ray elemental mapping (U, Si, and C) of ore samples performed on

Table 3 Values of geochemical ratios based on geochemical markers in unburnt and burnt sample extracts.

|                                 | % extract yields | <i>n</i> -Alkane maximum  | CPI <sub>total</sub> | CPI <sub>24–34</sub> | CPI <sub>17–23</sub> | OEP  | Pr/Ph | Aromaticity | MNR  | N     | P     | F     | MF   | Py   | PheOH |
|---------------------------------|------------------|---------------------------|----------------------|----------------------|----------------------|------|-------|-------------|------|-------|-------|-------|------|------|-------|
| <i>Unburnt coal</i>             |                  |                           |                      |                      |                      |      |       |             |      |       |       |       |      |      |       |
| Ry-1                            | 0.11             | <i>n</i> -C <sub>18</sub> | 1.09                 | 2.29                 | 1.42                 | 0.99 | 3.86  | 84.04       | 1.76 | 2.07  | 7.54  | 4.27  | 2.52 | –    | –     |
| Ry-2                            | 0.28             | <i>n</i> -C <sub>23</sub> | 1.02                 | 3.84                 | 1.25                 | 1.14 | 2.42  | 88.00       | 1.44 | –     | 17.96 | 10.38 | 9.59 | –    | –     |
| Ry-3                            | 1.14             | <i>n</i> -C <sub>16</sub> | 0.90                 | 1.89                 | 1.08                 | 0.66 | 4.08  | 88.19       | 1.65 | 6.84  | 11.75 | 4.45  | 4.20 | –    | –     |
| Ry-4                            | 1.33             | <i>n</i> -C <sub>13</sub> | 0.99                 | 3.45                 | 1.55                 | 0.96 | 1.65  | 62.68       | 1.06 | 6.48  | 10.06 | 2.01  | 1.07 | –    | –     |
| Ry-5                            | 0.68             | <i>n</i> -C <sub>13</sub> | 1.05                 | –                    | 1.42                 | 1.06 | 3.43  | 79.25       | 1.20 | 10.20 | 9.64  | 2.40  | 1.19 | –    | –     |
| Ry-7                            | 0.04             | <i>n</i> -C <sub>21</sub> | 0.94                 | 1.27                 | 1.47                 | 0.91 | –     | 83.56       | 0.89 | –     | 4.25  | 0.76  | –    | 1.90 | 0.91  |
| Ry-8                            | 0.02             | <i>n</i> -C <sub>19</sub> | 0.82                 | 1.3                  | 1.4                  | 0.98 | –     | 69.07       | 1.05 | –     | 2.87  | 0.47  | –    | 1.74 | 1.16  |
| <i>Burnt coal and claystone</i> |                  |                           |                      |                      |                      |      |       |             |      |       |       |       |      |      |       |
| Ry-9                            | 0.01             | –                         | 1.01                 | 1.57                 | 1.41                 | 0.95 | –     | 0.00        | –    | –     | –     | –     | –    | –    | –     |
| Ry-13/1                         | 0.04             | –                         | –                    | –                    | –                    | –    | –     | –           | –    | –     | –     | –     | –    | –    | –     |
| Ry-13/2                         | 0.01             | –                         | –                    | –                    | –                    | –    | –     | –           | –    | –     | –     | –     | –    | –    | –     |
| Ry-14/1                         | 0.01             | –                         | –                    | –                    | –                    | –    | –     | –           | –    | –     | –     | –     | –    | –    | –     |
| Ry-14/2                         | 0.02             | –                         | –                    | –                    | –                    | –    | –     | –           | –    | –     | –     | –     | –    | –    | –     |

Carbon preference index  $CPI_{total} = \sum \text{odd number} / \sum \text{even number}$ , m/z = 85 (Simoneit, 1989).

Carbon preference index  $CPI_{24–34} = 0.5 \{ [(n-C_{25} + n-C_{27} + n-C_{29} + n-C_{31} + n-C_{33}) / (n-C_{24} + n-C_{26} + n-C_{28} + n-C_{30} + n-C_{32})] + [(n-C_{25} + n-C_{27} + n-C_{29} + n-C_{31} + n-C_{33}) / (n-C_{26} + n-C_{28} + n-C_{30} + n-C_{32} + n-C_{34})] \}$ , m/z = 85 (Bray and Evans, 1961).

Carbon preference index  $CPI_{17–23} = 0.5 \{ [(n-C_{17} + n-C_{19} + n-C_{21}) / (n-C_{18} + n-C_{20} + n-C_{22})] + [(n-C_{19} + n-C_{20} + n-C_{23}) / (n-C_{18} + n-C_{20} + n-C_{22})] \}$ , m/z = 85 (Kotarba and Clayton, 2003).

Odd-over-even predominance  $OEP = (n-C_{21} + 6 * n-C_{23} + n-C_{25}) / (4 * n-C_{22} + 4 * n-C_{24})$ , m/z = 85 (Scalan and Smith, 1970).

Methylnaphthalene ratio  $MNR = 2\text{-methylnaphthalene} / 1\text{-methylnaphthalene}$ , m/z = 156 (Radke et al., 1982).

Pr/Ph = pristane/phytane; N - naphthalene; P - phenanthrene; F - fluoranthene; Py - pyrene; PheOH - phenanthrol.

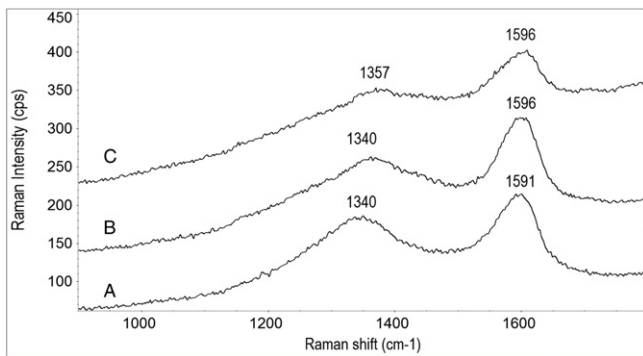


Fig. 8. Representative Raman spectra of coal sample Ry-5: A – halo with reflectance R = 2.42%, B – fusinite with reflectance R = 1.87%, C – collotelinite with reflectance R = 0.80%.

the electron microprobe indicated that not all U is in coffinite or uraninite (Smith, 1984). Some uranium may be adsorbed onto organic matter (Jennings and Leventhal, 1977; Borovec et al., 1979) at an early stage of coalification. However, using areal BSE mapping of our samples, finely dispersed uranium was not detected in individual macerals.

- (2) The origin of veinlet-type base metal mineralization in a small part of uranium in coal samples from the Novátor mine is more difficult to explain because the timing of this type of mineralization is difficult to assess. In the study area, up to 800 m of volcanic rocks with a small intercalation of sandstones and conglomerates form a hanging wall in the Rybníček coal seam (Fig. 2). The Autunian volcanic complex is composed of intermediate volcanic rocks from effusions, sills and intrusion bodies, whereas rhyolites consist mainly of ignimbrites (Suk, 1984). Small manifestations of base-metal, predominantly chalcopyrite mineralization are known at the basal part of the volcanic rocks pile (Bernard, 1991). It is, therefore, suggested that base metal hydrothermal mineralization in the coal samples may be related to Autunian volcanic and related hydrothermal processes. Within this scenario, not only geochemistry of coal but also coal physical properties (reflectance, Raman characteristics) and the composition of organic extracts may have been affected by both syngenetic uranium-, as well as epigenetic base metal mineralization.

5.2. Organic petrology and geochemistry of unburnt coal and its relationship to mineralization

Random reflectance values of vitrinite in coal from the unburnt zone of the Novátor mine waste dump varied between 0.72% and 0.86%. These reflectance values are high for Lower Permian bituminous coal

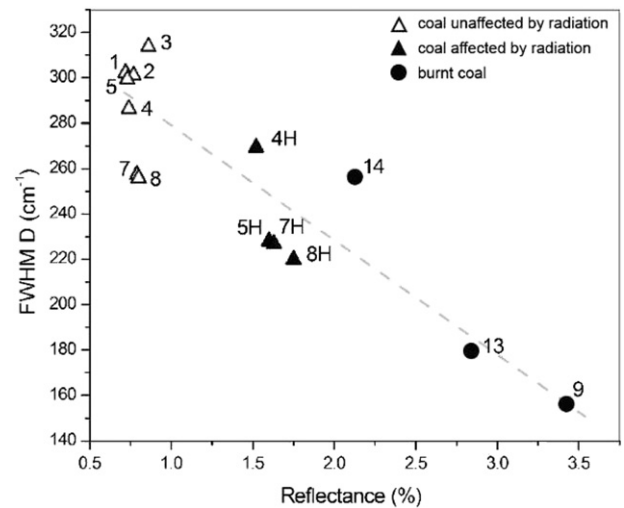
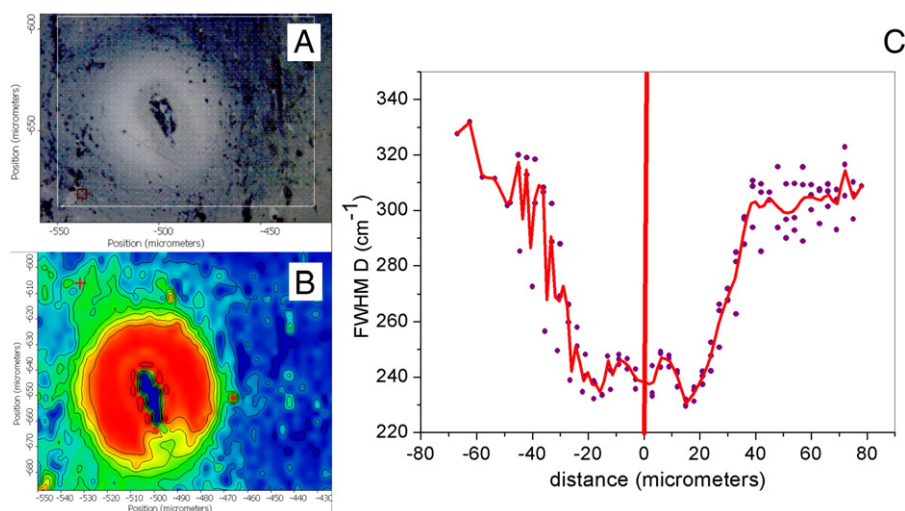


Fig. 9. Correlation between average reflectance and FWHM D of unburnt coal, radiation affected haloes (symbol H) and burnt coals.

and correspond to the rank of the underlying Upper Carboniferous coals mined in the Intra-Sudetic Basin ( $R_r = 0.68\text{--}1.20\%$ ; Opluštil et al., 2013). An unusually high rank of unburnt coal, loss of liptinite fluorescence, and the formation of fissures are typical changes in coal affected by intrusions or dykes in the neighbourhood of coal seams, as described by many authors, for example Kisch and Taylor (1966), Goodarzi and Cameron (1990), Murchison (2006), Amijaya and Littke (2006), Mastalerz et al. (2009). In addition to the increased reflectance of vitrinite and liptinite, numerous different-sized cracks perpendicular to the stratification, often filled with mineral phases, were found in many samples (see Section 4.1). Another anomaly is the occurrence of pseudovitrinite (Table 2) with typical short parallel slits and an increase in collotelinite reflectance that was also detected in small amounts (up to 3 vol.%) in the samples. Generally, the occurrence of pseudovitrinite can be the result of primary oxidation, drying or dessication during peat formation, post coalification oxidation processes, and/or stress caused by burial depth pressure or thermal stress (Benedict et al., 1968; Gurba and Ward, 1998; Kruszewska, 1998; Mastalerz and Drobnik, 2005). The described changes in optical properties of coal samples may be related to thermal stress induced by the thick volcanic pile forming the hanging wall of the Rybníček coal seam (Fig. 2). It could be accompanied by chemical changes in coal such as decreases in hydrogen, volatile matter, and aliphatic hydrocarbon compounds, an increase in organic matter aromaticity, and changes in inorganic geochemistry (Ward et al., 1989; Finkelman and Stracher, 2011).

Table 4  
Raman parameters of unburnt and burnt coal and claystone.

| Coal | Number of measure | D position average (cm <sup>-1</sup> ) | D positions interval (cm <sup>-1</sup> ) | FWHM D average (cm <sup>-1</sup> ) | FWHM D interval (cm <sup>-1</sup> ) | G position average (cm <sup>-1</sup> ) | G positions interval (cm <sup>-1</sup> ) | FWHM G average (cm <sup>-1</sup> ) | FWHM G interval (cm <sup>-1</sup> ) |
|------|-------------------|--|--|------------------------------------|-------------------------------------|--|--|------------------------------------|-------------------------------------|
| 1    | 5                 | 1348                                   | 1337–1353                                | 302                                | 229–341                             | 1593                                   | 1590–1598                                | 76                                 | 67–85                               |
| 2    | 7                 | 1347                                   | 1338–1354                                | 301                                | 240–339                             | 1593                                   | 1591–1598                                | 77                                 | 67–83                               |
| 3    | 5                 | 1352                                   | 1348–1356                                | 314                                | 263–354                             | 1592                                   | 1588–1596                                | 78                                 | 69–92                               |
| 4    | 13                | 1347                                   | 1334–1353                                | 286                                | 228–340                             | 1593                                   | 1591–1596                                | 78                                 | 68–80                               |
| 5    | 10                | 1347                                   | 1337–1354                                | 299                                | 259–341                             | 1593                                   | 1591–1595                                | 76                                 | 70–84                               |
| 7    | 10                | 1352                                   | 1341–1356                                | 257                                | 223–282                             | 1596                                   | 1596–1599                                | 73                                 | 59–80                               |
| 8    | 12                | 1353                                   | 1340–1357                                | 256                                | 206–275                             | 1596                                   | 1595–1600                                | 74                                 | 61–80                               |
| 9    | 4                 | 1347                                   | 1340–1351                                | 156                                | 123–177                             | 1598                                   | 1597–1599                                | 90                                 | 80–96                               |
| 13   | 6                 | 1349                                   | 1345–1353                                | 179                                | 161–203                             | 1593                                   | 1589–1596                                | 91                                 | 89–94                               |
| 14   | 9                 | 1354                                   | 1351–1356                                | 256                                | 226–265                             | 1599                                   | 1598–1600                                | 74                                 | 70–78                               |
| 4H   | 5                 | 1348                                   | 1342–1353                                | 269                                | 250–294                             | 1594                                   | 1592–1595                                | 78                                 | 77–79                               |
| 5H   | 4                 | 1336                                   | 1333–1339                                | 228                                | 228–228                             | 1592                                   | 1591–1593                                | 82                                 | 77–86                               |
| 7H   | 4                 | 1341                                   | 1339–1343                                | 227                                | 221–234                             | 1592                                   | 1592–1593                                | 83                                 | 81–85                               |
| 8H   | 4                 | 1338                                   | 1335–1340                                | 220                                | 215–224                             | 1593                                   | 1591–1593                                | 86                                 | 83–87                               |



**Fig. 10.** Micrograph of an area in a polished section from the coal sample Ry-5 chosen for Raman microspectroscopy mapping (A), correlation map of halo (B) and development of the FWHM D values across the halo (C).

The character of the *n*-alkane distribution was unusual for typical coal samples that have mainly long-chain *n*-alkanes from plant waxes with odd-over-even predominance. Various parameters are used to study geochemical samples to differentiate *n*-alkane sources as being of biogenic, petrogenic or anthropogenic origins. The values of the OEP and CPI indices used (Table 4) exhibited non-typical values for bituminous coal, which means that the samples were, in some way, thermally affected. There were actually several types of *n*-alkane distributions: a distribution with abundances over the whole range, a narrower distribution of short-chain *n*-alkanes with *n*-C<sub>13</sub>–*n*-C<sub>16</sub> predominance, and a distribution of middle chain *n*-alkanes with *n*-C<sub>19</sub>–*n*-C<sub>25</sub> predominance. Although the *n*-alkanes occurred within variable ranges and abundance, generally these types of distributions reflected processes connected with various degrees of heating, pressure, radiolysis, or leaching. Furthermore, the possible input of pyrolysate migration within the dump, and mixing of migrating pyrolysates with coaly bitumen present in situ cannot be ignored.

Similarly, these processes affected the presence of pristane and phytane within the samples: the absence of pristane and phytane in the sample extracts of Type II are evidence of higher heating, leaching or radiolytic effects. The Pr/Ph ratio is a widely used biomarker for assessment of redox conditions during sediment accumulation (Didyk et al., 1978; ten Haven et al., 1987). However, this ratio cannot imply the degree of oxidation, in the case of redeposited or affected coal samples, because it is sensitive to thermal and radiolytic alteration (Havelcová et al.,

2014). Coal wastes showed higher values of Pr/Ph upon heating (Miszkennan and Fabiańska, 2010). The Pr/Ph values for samples classified as Type I were higher than the values typical for coals, and a low degree of degradation of these materials is assumed.

Different distributions of alkylated PAHs with 2–4 aromatic rings were also identified, in comparison with Type 1. Although the identified PAHs corresponded to high rank coals, where the condensed network created smaller and more stable molecules in the mobile and extractable phases (Stout and Emsbo-Mattingly, 2008), their distribution was affected by processes within the dump.

Phenolic compounds are used as a signature of coal-waste self-heating (Nádudvari and Fabiańska, 2016) as they are derived from the thermal destruction of vitrinite macromolecules (Hatcher and Clifford, 1997). They are abundant in pyrolytic products of coal. In the samples studied, only phenanthrol, the oxidized product from the reaction of phenanthrene with OH radicals (Lee and Lane, 2010) was identified in Type 2 sample extracts. Usually coal-waste extracts comprise phenol and cresols, and other phenols occur in lower amounts (Miszkennan and Fabiańska, 2011) so the presence of phenanthrol most probably indicates that hydrothermal or thermal evaporation of lighter compounds affected the samples.

Generally, chemical substances identified in the sample extracts can be interpreted as: 1) products of chemical transformations of biological precursors during diagenesis and catagenesis in the original coal, 2) products of thermally or radiolytically altered organic matter and, 3) products of bitumen migration from heated zones in the accumulated matter, adsorbed on coal or washed with water.

In samples Ry-4, Ry-7, Ry-8 with high uranium contents ( $U > 1000$  ppm) the effects of radiation on coal properties were exhibited in numerous high-reflectance haloes adjacent to grains of uranium minerals. Values of the FWHM D were also higher in radiation-induced haloes compared to bulk organic matter, and IR spectra confirmed that alterations in haloes resulted in radiolytic cleavage of aliphatic structures to form esters (1474 cm<sup>-1</sup>), carboxylic acids and alkanols. This agreed with results of Havelcová et al. (2014) who found that  $\alpha$ -ray flux from uranium minerals involves dehydrogenation and oxidation, mainly of aliphatic, aromatic and hydroxyl structures, and an increase in aromaticity and ether bonds in sub-bituminous coal from the Sokolov Basin, Czech Republic. Furthermore, an increase in the spectral features at 880–900 cm<sup>-1</sup> was observed in radiation-induced haloes compared with radiation unaffected coal from the Novátor mine (Fig. 11). Vibrations in this part of the spectra can be assigned to antisymmetric U–O stretching and probably exchange of uranyl (UO<sub>2</sub><sup>+</sup>) ions. The bands of anti-symmetric stretching vibrations

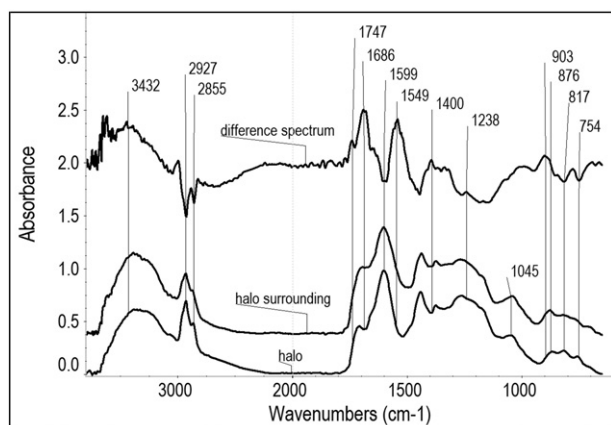


**Fig. 11.** ATR-FTIR microspectra of halo, halo surround and the difference spectrum (coal sample Ry-5).

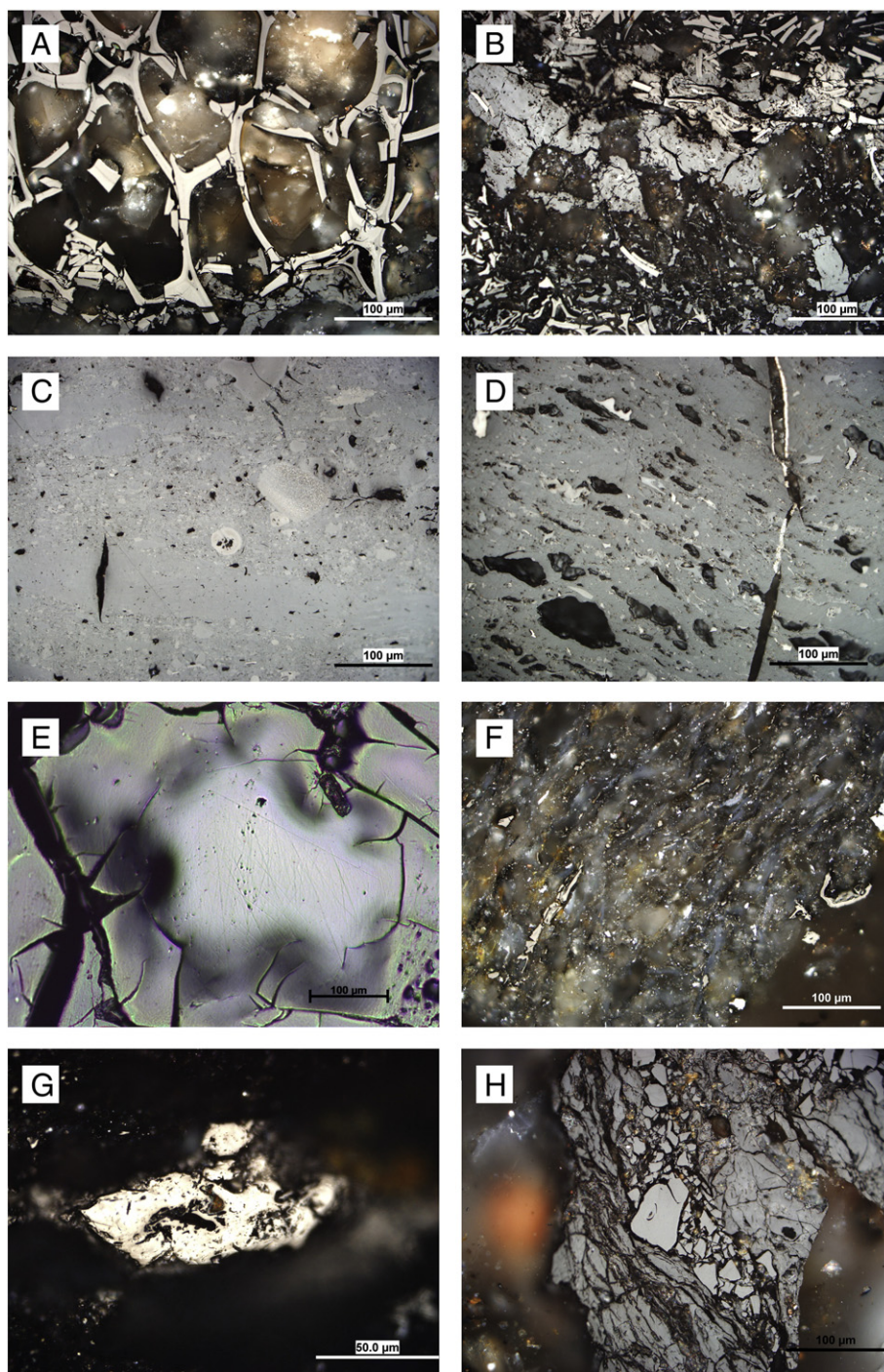


**Fig. 12.** Photomicrographs of organic matter in coal and claystone samples affected by self-ignition. A: High reflectance fusinite in carbonate. Sample Ry-14. B: Altered vitrinite band with cracks and fine pores between fusinite fragments in carbonate. Sample Ry-14/1. C: Massive texture of coke formed by high reflectance collotelinite and collodetrinite with light inertinite macerals. Sample Ry-14/2. D: Dense texture of coke formed by altered vitrinite mater with dispersed inertinite fragments and pores after degassing of liptinite. Sample Ry-14/1. E: Fragment of weathered solid bitumen particle with high relief. Sample Ry-14/2. F: Burnt claystone with disseminated fine high reflectance particles. Sample Ry-13/1. G: Detail of dense coke particles in sample Ry-9. H: Brecciated coal particle formed by altered vitrinite macrinite and inertodetrinite. Sample Ry-9. Photomicrographs A, B, C, D, F, G and H were taken in reflected white light using an immersion lens and photomicrograph E using a dry lens with 20× magnification.

of  $\text{—COO—}$  groups are situated in the region  $1560\text{--}1560\text{ cm}^{-1}$  and bands of the antisymmetric stretching vibration of  $\text{—COO—}$  groups in the region  $1400\text{--}1330\text{ cm}^{-1}$  (Koglin et al., 1978). In the difference spectrum, one positive band at  $876\text{ cm}^{-1}$ , and two negative bands at  $817$  and  $754\text{ cm}^{-1}$  can be seen, which can be assigned to the out-of-plane vibrations of C—H bonds of isolated, two and four adjacent hydrogens in the aromatic substituted system (Ibarra et al., 1996). The number of adjacent hydrogens per ring provides an estimation of the degree of aromatic substitution and condensation with increasing coalification.

Other than radiation-induced haloes, it is difficult to determine whether differences in the composition of bulk organic matter are due to radiation effects or differences in (hydro) thermal stress associated with volcanic activity and associated epigenetic mineralization. In natural systems, the effect of radiolytic alteration, at a molecular level can be attributed to reduced amounts of isoprenoids versus  $n$ -alkanes, decreased abundance of long chain alkanes and alkylated PAHs, increased aromaticity or unusual distributions of aromatic hydrocarbons (Havelcová et al., 2014; Court et al., 2006; Dahl et al., 1988). However,

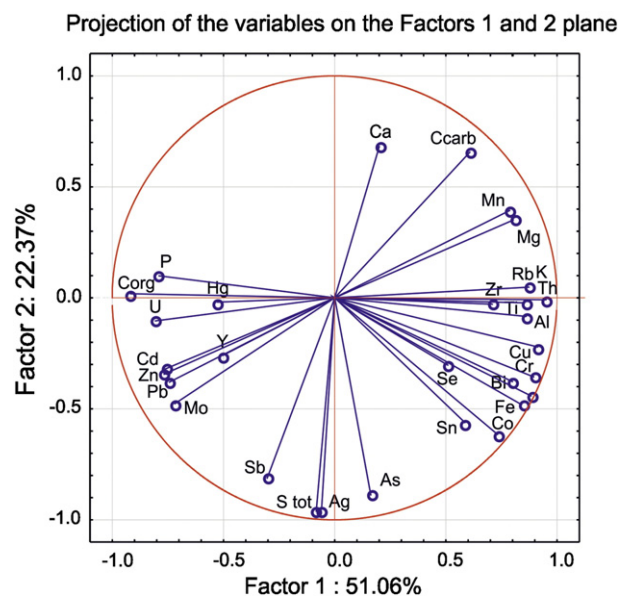


Fig. 13. Results of principal component analysis of burning-unaffected coal samples. Projection of the variables on the plane of factors 1 and 2. Number of samples: Ry-5.

it is possible to observe the same changes with increasing thermal stress related to various types of epigenetic, predominantly copper mineralization (Greenwood et al., 2013). Due to the combination of processes of heating, pressure, radiolysis or leaching together with pyrolysate migration and precipitation within a dump, it is difficult to estimate the contribution of radiolytic effects on the organic matter of samples.

Usually, aromatic hydrocarbon distributions are potentially useful in applied geochemistry, using various ratios and indices to evaluate thermal maturity of organic matter, and degradation of aromatic hydrocarbons. There are many ratios applied (Radke, 1988), however in this study, only the methyl-naphthalene ratio (MNR) was used because other ratios and indices were not possible to calculate or they did not show feedback. The MNR ratio is based on the distribution of methyl-naphthalene isomers caused by either selective generation of 2-methyl-naphthalene and/or selective transformation of 1-methyl-naphthalene. The ratio increases with maturity and usually dominates up to a vitrinite reflectance of 0.9% (Radke et al., 1982). However, to evaluate the maturity or degradation is problematic in the case of waste samples, and the ratio was used only to assess the samples. The calculated values showed a significant correlation with uranium content (Fig. 14). Misz et al. (2007) found a correlation between MNR and the vitrinite content for samples from coal wastes exposed to fire; however it is clear that this parameter also reflects radiolytic alterations.

No other significant differences between samples associated with higher uranium content were found, and it seems that the presence of uranium induces changes that are equivalent to those that occur during thermal degradation of organic matter. Significant correlations were also found between uranium content and average values of reflectance in individual samples.

### 5.3. Changes in organic components induced by self-burning

At the Novátor mine, coal and claystones vitrinite reflectance, morphology and compositions of various forms of self-burnt organic matter and various chemical indices were recorded. Variabilities in optical properties, and the composition and morphology of burnt organic matter are attributed to the resistance of organic particles to thermal treatment. Self-heating, spontaneous combustion, pyrolysis, anhydrous and hydrous pyrolysis are the most important transformation processes of both organic and mineral matter in coal wastes deposited in dumps. The scale of these processes depends on the properties of the maceral,

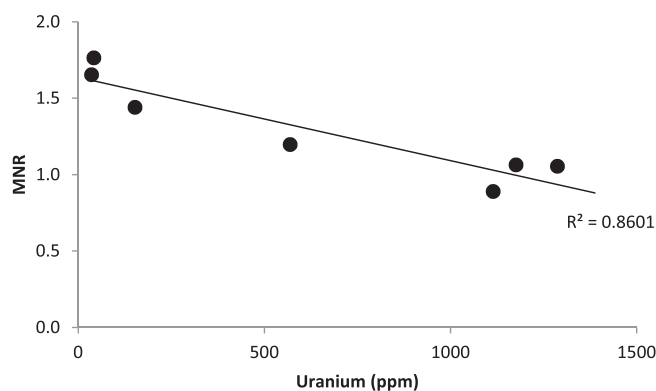


Fig. 14. Relationship between the MNR and uranium concentration.

mineral composition, rank of coal, and the heating history: heating time, temperature, rate, air access, and the presence of water (Taylor et al., 1998; Suárez-Ruiz and Crelling, 2008; Beamish et al., 2001; Beamish and Arisoy, 2007; Misz et al., 2007; Kus et al., 2010; Misz-Kennan and Fabiańska, 2010; Ribeiro et al., 2011, 2016). The results summarized in Table 2 and Fig. 12 documented a greater susceptibility of vitrinite and liptinite to thermal processes in burnt samples. Average reflectance values of vitrinite in samples Ry-14/1-2 increased by up to 1.31% and 1.77% respectively in altered coal matter with fissures, rare reaction rims and vitritized liptinite, and increased up to 2.13% and 2.26% in coke particles. Reflectance values of self-ignition altered coal matter and the resulting coke corresponded to moderately and strongly altered wastes, as classified by Misz-Kennan and Fabiańska (2011). These authors distinguished three types of alteration of wastes in the Starzykowice dump: 1) unaltered waste with highest contents of unaltered macerals; 2) moderately thermally-altered wastes of reflectance 0.6–1.6% with considerable amounts of oxidized vitrinite; 3) strongly altered wastes with strongly altered organic matter of reflectance 1.86–5.42%. Unaltered wastes were not found in self-burnt zones in the Novátor mine dump. Coal matter heated slowly at a low temperature for a long time showed cracks, paler colour of vitrinite and liptinite and reaction rims. Liptinite then disappeared and organic matter became strongly thermally altered, displaying high reflectance (Fig. 12B, C). Increasing rates of heating caused an increased tendency to soften, release gas, form pores and generate optical anisotropy. Weak mosaic optical anisotropy, and the occurrence of fissures and pores after degassing of liptinite macerals, corresponded with a weakly developed coke texture, and suggests that the temperature did not exceed 500 °C, according to Singh et al. (2007), Mastalerz et al. (2009), and Misz et al. (2007). The absence of liptinite macerals indicates that the temperature of thermal stress was higher than 300 °C (Mastalerz and Mastalerz, 2000). The macerals of the inertinite group showed little change in morphology and a significant increase in reflectance (Fig. 12C and D) under similar thermal conditions. More reflecting inertinite did not fuse during carbonization and combustion, and formed isotropic coke with an average reflectance of up to 2.65%, which was observed in all burnt samples similar to bitumen drops and fillings.

The lowest carbon contents were found in strongly thermally altered claystones of samples Ry-9 and Ry-13/1-2 with pores and disseminated amounts of small carbonaceous charred particles up to 100 µm. Average reflectance values of isotropic coke particles of dense, massive and rare networks texture,  $R = 3.59\text{--}4.52\%$  were higher than rare bitumen drops and fillings of fine fissures and cracks.

The intensity ratios, position and the FWHMs of the D and G band can be used as indicators of char and maceral structural order (Sheng, 2007; Guedes et al., 2010). The Raman spectroscopy results in Fig. 9 show that samples Ry-1, Ry-2 and Ry-3 from the study collection with very low uranium contents ( $U = 42.2, 152.7, \text{ and } 35.8 \text{ ppm}$ , respectively), had the lowest degree of coalification. On the other hand, claystone

samples Ry-13 and Ry-9 with a similar uranium content ( $U = 60.1, 99.5$  ppm) had the smallest FWHM D ( $179$  and  $156 \text{ cm}^{-1}$ ) values and therefore higher coalification, predominantly due to thermal degradation of the coal samples.

The burnt samples were almost totally reduced in organic content. Due to oxidation, in combination with an oxygen-free environment where heat was released, organic matter was combusted and pyrolysed, and carbon and hydrogen content were decreased (Table 1). The results obtained from GC/MS analyses of sample extracts reflect the maceral compositions of the self-ignition affected samples: altered vitrinite, higher content of inertinite and rare liptinite macerals. The structure of the vitrinite maceral group is generally characterized by the presence of short aliphatic chains and rising aromatization of the macromolecular structure, reflecting the coal rank (Li et al., 2013). This structure undergoes changes during combustion, resulting in the release of organic fractions, followed by rearrangements, cyclizations or radical condensation reactions leading to more aromatic structures (Mastral and Callén, 2000). Vitrinite, modified during the thermal process yielded an altered form with cracks, higher reflectance and a more ordered structure approaching the highly carbonised material of the inertinite maceral group. Incomplete combustion and decomposition caused the production of fragments with the aromatic structure of the coal, and phenanthrene is the product of this reaction, with benzotriazole being the pyrolytical product.

## 6. Conclusions

Uranium and base metal mineralized coal from the former Novátor mine waste pile was partly affected by self-burning processes. Disseminated uranium minerals caused local radioactive alterations of the coal matrix. The diameter of the rounded radiation-induced haloes ranged from  $35$  to  $100 \mu\text{m}$ . Radiation alteration was nonhomogeneous and was manifested by higher reflectance and lower values of Raman band disorder (D) in contact with the uranium mineral grain relative to radiation-affected organic components of coal. The infrared spectroscopy revealed lower amounts of aliphatic C—H and hydroxyl bonds relative to the radiation-affected coal matrix. However, the geochemical compositions of extractable hydrocarbons from bulk coal were very variable and did not correspond to the contents of uranium and base metals in individual samples, with the exception of the MNR ratio. Its values being in the range  $0.89$ – $1.76$ , corresponding well to uranium concentrations in the bulk samples, suggesting that the presence of radionuclides may have an impact on the chemical composition and structural ordering of organic matter similar to thermal alteration.

Variations in reflectance values and the composition of organic extracts in unburnt samples may be explained as being due to primary heterogeneity of coal, radiation-induced changes and/or by various degrees of thermal stress related to the emplacement of Lower Permian volcanic rocks that form a hanging wall in the Rybníček coal seam. Base-metal mineralization was confined to fissures orientated perpendicularly to coal stratification and is most probably related to volcanic activity. The hydrothermal alteration is manifested by the higher vitrinite reflectance values, the occurrence of pseudovitrinite and the weak fluorescence intensity of liptinite at the vicinity of mineralized veinlets.

In self-ignition-affected samples, reflectance and organic-geochemical characteristics of coal mirrored the intensity of the burning processes. Organic matter in steam-affected samples collected adjacent to a burnt-out part of the waste pile show high reflectance of porous and cracked vitrinite and occurred in association with coke and rare bitumen. Clasts of altered coal comprised fine porous and cracked vitrinite, inertinite, liptinite without fluorescence, fusinite impregnated by carbonate, rare coke and solid bitumens. The occurrence of authigenic hydrous aluminosilicates indicates a high partial pressure of water (hydrolysis). In the burnt-out zone itself, only fine-sized high reflecting

coke particles prevailed, and solid bitumen was rare. After cessation of coal burning, samples were, to various degrees, affected by weathering.

The results revealed that during self-burning, a range of chemical elements, notably U, Pb, Cu, Zn and Cd and phenols accumulated in the burnt-out part of the dump. These components represent a potential hazard to the environment, especially for local watershed, soil and vegetation. Therefore, data summarized in this study can be used to explain mechanisms and degrees of leaching of potentially harmful elements in subsequent environmental studies.

## Acknowledgements

This study was supported by the Czech Science Foundation grant 15-11674S “A model of mobilization and geochemical cycles of potentially hazardous elements and organic compounds in burned coal heaps”. Our thanks to the Operational Program Prague - Competitiveness, project “Centre for Texture Analysis” (No. CZ.2.16/3.1.00/21538), and the long-term conceptual development of the research organization RVO: 67985891. Technical support in the field was provided by V. Majer, F. Veselovský and J. Malec (Czech Geological Survey) and is greatly appreciated. F. Laufek (Czech Geological Survey) is thanked for the interpretation of X-ray diffraction analysis of inorganic components of coal and N. Mészárosová (Geological Institute, Academy of Sciences of the Czech Republic), R. Škoda (Masaryk University in Brno), M. Žaloudková and L. Borecká (Institute of Rock Structure and Mechanics Academy of Sciences of the Czech Republic) for performing microprobe analyses. The authors are grateful to John Brooker for reviewing and correcting the manuscript.

## References

- Adamec, Z., 2015. Mining at the Žacléf Region. Pratr Publishing House, Trutnov, Czech Republic, p. 158.
- Amijaya, H., Littke, R., 2006. Properties of thermally metamorphosed coal from Tanjung Enim Area, South Sumatra basin, Indonesia with special reference to the coalification path of macerals. *Int. J. Coal Geol.* 66, 271–295.
- Arapov, J.A., Bojcov, V.J., Česnokov, N.J., Djakonov, A.V., Halbrštát, J., Jakovjenko, A.M., Kolek, M., Komínek, J., Kozyrev, V.N., Kremčukov, G.A., Lažanský, M., Milovanov, I.A., Nový, V., Šorf, F., 1984. Czechoslovak Uranium Deposits. Czechoslovak Uranium Industry, Příbram, p. 363 in Czech with English summary.
- Bailey, J.G., Tate, A., Diessel, C.F.K., Wall, T.F., 1990. A char morphology system with applications to coal combustion. *Fuel* 69, 2258–239.
- Beamish, B.B., Arisoy, A., 2007. Effects of mineral matter on coal self-heating rate. *Fuel* 87, 125–130.
- Beamish, B.B., Barakat, M.A., St. George, J.D., 2001. Spontaneous-combustion propensity of New Zealand coals under adiabatic conditions. *Int. J. Coal Geol.* 45, 217–224.
- Benedict, L.G., Thompson, R.R., Shigo, J.J., Aikman, I.R.P., 1968. Pseudovitrinite in Appalachian coking coals. *Fuel* 47, 125–143.
- Bernard, J.H., 1991. Empirical Types of Ore Mineralizations in the Bohemian Massif. Czech Geological Survey, Prague 80-7075-006-5, p. 181.
- Borovec, Z., Kříbek, B., Tolar, V., 1979. Sorption of uranyl by humic acids. *Chem. Geol.* 27, 39–46.
- Bray, E.E., Evans, E.D., 1961. Distribution of n-paraffins as a clue to recognition of source beds. *Geochim. Cosmochim. Acta* 22, 2–15.
- Ciesielczuk, J., Misz-Kennan, M., Hower, J.C., Fabiańska, M.J., 2014. Mineralogy and geochemistry of coal wastes from the Starzykowice coal-waste dump (Upper Silesia, Poland). *Int. J. Coal Geol.* 127, 42–55.
- Court, R.W., Sephton, M.A., Parnell, J., Gilmour, I., 2006. The alteration of 506 organic matter in response to ionising irradiation: chemical trends and implications for extraterrestrial sample analysis. *Geochim. Cosmochim. Acta* 70, 1020–1039.
- Dahl, J., Hallberg, R., Kaplan, I.R., 1988. Effects of irradiation from uranium decay on extractable organic matter in the Alum Shales of Sweden. *Org. Geochem.* 12, 559–571.
- Didyk, B.M., Simoneit, B.R.T., Brasse, S.C., Eglinton, G., 1978. Organic geochemical indicators of paleoenvironment conditions of sedimentation. *Nature* 272, 216–222.
- Dill, H., 1983. First occurrences of some uranium minerals and sulfides in the uranium exploration sites of N. Bavaria. *N. Jb. Mineral. Abh.* 147, 184–190.
- Dill, H., Koch, J., Tescher, M., Wehner, H., 1991. Permo-Carboniferous beds in the Stockheim Basin/NE-Bavaria. *Erdoel Kohle Erdgas Petrochem.* 44, 97–105.
- Emsbo-Mattingly, S.D., Stout, S.A., 2011. Semivolatile hydrocarbon residues of coal and coal tar. In: Stracher, G.B., Prakash, A., Sokol, E. (Eds.), *Coal and Peat Fires: A Global Perspective* – Geology and Combustion vol. 1. Elsevier, Amsterdam-Boston-Heidelberg, pp. 173–209.
- Finkelman, R.B., 2004. Potential health impacts of burning coal beds and waste banks. *Int. J. Coal Geol.* 51, 19–24.
- Finkelman, R.B., Stracher, G.B., 2011. Environmental and health impacts of coal fires. In: Stracher, G.B., Prakash, A., Sokol, E.V. (Eds.), *Coal and Peat Fires: A Global Perspective* – 7. Elsevier, Amsterdam, pp. 115–125.

- Fuchs, L.H., Hoekstra, H.R., 1959. The preparation and properties of uranium (IV) silicate. *Am. Mineral.* 44, 1057–1063.
- Glickson, M., Mastalerz, M. (Eds.), 2000. *Organic Matter and Mineralization: Thermal Alteration, Hydrocarbon Generation and Role in Metallogenesis*. Kluwer Academic Publishers, Dordrecht 420 pp.
- Goodarzi, F., Cameron, A., 1990. Organic petrology and elemental distribution in thermally altered coals from Telia, British Columbia. *Energy Sources* 315–343.
- Greenwood, P.F., Brocks, J.J., Grice, K., Schwark, L., Jaraula, C.M.B., Dick, J.M., Evans, K.E., 2013. Organic geochemistry and mineralogy. I. Characterization of organic matter associated with metal deposits. *Ore Geol. Rev.* 50, 1–27.
- Guedes, A., Valentim, B., Prieto, A.C., Rodrigues, S., Noronha, F., 2010. Micro-Raman spectroscopy of collotelinite, fusinite and macrinite. *Int. J. Coal Geol.* 83, 415–422.
- Gurba, L.W., Ward, C.R., 1998. Vitrinite reflectance anomalies in the high-volatile bituminous coals of the Gunnedah Basin, New South Wales, Australia. *Int. J. Coal Geol.* 36, 111–140.
- Halbach, P., von Borstel, D., Janetzke, A., 1984. Carburan oxide in Lower Permian high volatile bituminous coal. *Naturwissenschaften* 7, 41–42.
- Hatcher, P.G., Clifford, D.J., 1997. The organic geochemistry of coal: from plant materials to coal. *Org. Geochem.* 27, 251–274.
- Havelcová, M., Machovič, V., Mizera, J., Sýkorová, I., Borecká, L., Kopecký, L., 2014. A multi-instrumental geochemical study of anomalous uranium enrichment in coal. *J. Environ. Radioact.* 137, 52–63.
- Ibarra, J.V., Muñoz, E., Moliner, R., 1996. FTIR study of the evolution of coal structure during the coalification process. *Org. Geochem.* 24, 725–735.
- ICCP, 1998. The new vitrinite classification (ICCP system 1994). *Fuel* 77, 349–358.
- ICCP, 2001. The new inertinite classification (ICCP system 1994). *Fuel* 80, 459–471.
- ISO 1171:2010, Solid mineral fuels — determination of ash (16 pp.).
- ISO 5069-2:1983, Brown coals and lignites — principles of sampling — part 2: sample preparation for determination of moisture content and for general analysis (12 pp.).
- ISO 609:1996, Solid mineral fuels — determination of carbon and hydrogen - high temperature combustion method (16 pp.).
- ISO 7404-3, 2009. Methods for the Petrographic Analysis of Coal – Part 3: Method of Determining Maceral Group Composition. International Organization for Standardization, Geneva, Switzerland 14 pp.
- ISO 7404-5, 2009. Methods for the Petrographic Analysis of Coal – Part 5: Method of Determining Microscopically the Reflectance of Vitrinite. International Organization for Standardization, Geneva, Switzerland 14 pp.
- Jennings, J.K., Leventhal, J.S., 1977. A new structural model for humic material which shows sites for attachment of oxidized uranium species. In: Campbell, J.A. (Ed.), *Short Papers of the US Geological Survey Uranium-Thorium Symposium*. US Geol. Surv. Circ Vol. 753, pp. 10–11.
- Kisch, H.J., Taylor, G.H., 1966. Metamorphism and alteration near an intrusive contact. *Econ. Geol.* 61, 343–361.
- Kochenov, A.V., Korolev, V.T., Dubinchuk, V.T., Medvedev, Y.L., 1977. Experimental data on the conditions of precipitation of uranium from aqueous solutions. *Geochem. Int.* 14, 82–87.
- Koglin, E., Schenk, H.J., Schwochau, K., 1978. Spectroscopic studies on the binding of uranium by brown coal. *Appl. Spectrosc.* 32, 486–488.
- Kotarba, M.J., Clayton, J.L., 2003. A stable carbon isotope and biological marker study of Polish bituminous coals and carbonaceous shales. *Int. J. Coal Geol.* 55, 73–94.
- Křibek, B., Podlaha, J., 1980. The stability constant of the  $\text{UO}_2^{2+}$ -humic acid complex. *Org. Geochem.* 2, 93–97.
- Křibek, B., Žák, K., Spangenberg, J., Jehlička, J., Prokeš, S., Komínek, J., 1999. Bitumens in the late Variscan hydrothermal vein-type uranium deposits of Příbram, Czech Republic: sources, radiation-induced alteration, and relation to mineralization. *Econ. Geol.* 94, 1093–1114.
- Kruszewska, K.J., 1998. The reactivity of pseudovitrinite in some coals. *Fuel* 77, 1655–1661.
- Kus, J., Kaufhold, S., Klosa, D., Jianwei, M., Schmidt, M., Suhendra, 2010. Coal fire geothermometer: controlling the extent and temperature field of underground coal fire zones. In: Drebenstedt, C., Fischer, C., Meyer, U., Jianjun, W., Bing, K. (Eds.), *Latest Developments in Coal Fire Research. Bridging the Science, Economics, and Politics of a Global Disaster*. ICCFR2, 19–21 May 2010, DBB Forum Berlin. TU Bergakademie Freiberg, Germany, pp. 75–85.
- Kwicińska, B., Petersen, H.I., 2004. Graphite, semigraphite, natural coke, and natural char classification – ICCP system. *Int. J. Coal Geol.* 67, 99–116.
- Landais, P., 1993. Bitumens in uranium deposits. In: Parnell, J., Kucha, H., Landais, P. (Eds.), *Bitumens in Ore Deposits*. Springer-Verlag, Berlin, Heidelberg New York, pp. 213–238.
- Landais, P., 1996. Organic geochemistry of sedimentary uranium ore deposits. *Ore Geol. Rev.* 11, 33–51.
- Lee, J., Lane, D.A., 2010. Formation of oxidized products from the reaction of gaseous phenanthrene with the OH radical in a reaction chamber. *Atmos. Environ.* 44, 2469–2477.
- Lester, E., Alvarez, D., Borrego, A.G., Valentim, B., Flores, D., Clift, D., Rosenberg, P., Kwicińska, B., Barranco, R., Petersen, H.I., Mastalerz, M., Milenkova, K.S., Panaitescu, C., Marques, M.M., Thompson, A., Watts, D., Hanson, S., Predanu, G., Misz, M., Wu, T., 2010. The procedure used to develop a coal char classification – Commission III Combustion Working Group of the International Committee for Coal and Organic Petrology. *Int. J. Coal Geol.* 81, 333–342.
- Leventhal, J.S., Daws, T.A., Frye, J.S., 1986. Organic geochemical analysis of sedimentary organic matter associated with uranium. *Appl. Geochem.* 1, 241–249.
- Lewan, M.D., Buchardt, B., 1989. Irradiation of organic matter by uranium decay in the Alum Shale, Sweden. *Geochim. Cosmochim. Acta* 53, 1307–1322.
- Li, W., Zhu, Y., Chen, S., Zhou, Y., 2013. Research on the structural characteristics of vitrinite in different coal ranks. *Fuel* 107, 647–652.
- Mastalerz, M., Drobnik, A., 2005. Optical properties of pseudovitrinite: implications for its origin. *Int. J. Coal Geol.* 62, 250–258.
- Mastalerz, M., Mastalerz, K., 2000. Volcanic and post-volcanic hydrothermal activity in the Intrasudetic Basin, SW Poland: implications for mineralization. In: Glickson, M., Mastalerz, M. (Eds.), *Organic Matter and Mineralization: Thermal Alteration, Hydrocarbon Generation and Role in Metallogenesis*. Kluwer Academic Publishers, Dordrecht, pp. 185–203.
- Mastalerz, M., Drobnik, A., Schimmelmann, A., 2009. Changes in optical properties, chemistry, and micropore and mesopore characteristics of bituminous coal at the contact with dikes in the Illinois Basin. *Int. J. Coal Geol.* 77, 310–319.
- Mastral, A.M., Callén, M.S., 2000. A review on polycyclic aromatic hydrocarbon (PAH) emissions from energy generation. *Environ. Sci. Technol.* 34, 3051–3057.
- Misz, M., Fabiańska, M., Cmiel, S., 2007. Organic components in thermally altered coal waste: preliminary petrographic and geochemical investigation. *Int. J. Coal Geol.* 71, 405–424.
- Misz-Kennan, M., Fabiańska, M.J., 2010. Thermal transformation of organic matter in coal waste from Rymer Cones (Upper Silesian Coal Basin, Poland). *Int. J. Coal Geol.* 81, 343–358.
- Misz-Kennan, M., Fabiańska, M.J., 2011. Application of organic petrology and geochemistry to coal waste studies. *Int. J. Coal Geol.* 88, 1–23.
- Misz-Kennan, M., Kus, J., Flores, D., Avila, C., Christianis, K., Hower, J., Kalaitzidis, S., O'Keefe, J., Marques, M., Pusz, S., Ribeiro, J., Suárez-Ruiz, I., Sýkorová, I., Wagner, N., Životić, D., 2009. Report of the 2009 round robin exercise of the self-heating of coal and coal wastes working group. ICCP News 48, 68–60.
- Murchison, D., 2006. The influence of heating rates on organic matter in laboratory and natural environments. *Int. J. Coal Geol.* 67, 145–157.
- Náduvvari, Á., Fabiańska, M.J., 2016. The impact of water-washing, biodegradation and self-heating processes on coal waste dumps in the Rybnik Industrial Region (Poland). *Int. J. Coal Geol.* 154–155, 286–299.
- Opluštil, S., Edress, N.A., Sýkorová, I., 2013. Climatic vs. tectonic controls on peat accretion in non-marine setting; an example from the Zacléf Formation (Yeadonian-Bolsovian) in the Intra-Sudetic Basin (Czech Republic). *Int. J. Coal Geol.* 116–117, 135–157.
- Parnell, J., Kucha, H., Landais, P. (Eds.), 1993. *Bitumens in Ore Deposits*. Springer-Verlag, Berlin – Heidelberg – New York 520 pp.
- Pešek, J., Sýkorová, I., Jelínek, E., Michna, O., et al., 2010. Major and Minor Elements in the Hard Coal From the Czech Upper Paleozoic Basins. Prague, Czech Geological Survey 978-80-7075-741-3, p. 40.
- Pone, J.D.N., Hein, K.A.A., Stracher, G.B., Annegarn, H.J., Finkelman, R.B., Blake, D.R., McCornack, J.K., Schroeder, P., 2007. The spontaneous combustion of coal and its by-products in the Witbank and Sasolburg coalfields of South Africa. *Int. J. Coal Geol.* 72, 124–140.
- Querol, X., Zhuang, X., Font, O., Izquierdo, M., Alastuey, A., Castro, I., van Drooge, B.L., Moreno, T., Grimalt, J.O., Elvira, J., Cabanas, M., Bartroli, R., Hower, J.C., Ayora, C., Plana, F., López Soler, R., 2011. Influence of soil cover on reducing the environmental impact of spontaneous coal combustion in coal waste gobs: a review and new experimental data. *Int. J. Coal Geol.* 85, 2–22.
- Radke, M., 1988. Application of aromatic compounds as maturity indicators in source rocks and crude oils. *Mar. Pet. Geol.* 5, 224–236.
- Radke, M., Willsch, D.H., Leythaeuser, D., 1982. Aromatic components of coal: relation of distribution pattern to rank. *Geochim. Cosmochim. Acta* 46, 1831–1848.
- Ribeiro, J., Ferreira da Silva, E., Flores, D., 2010. Burning of coal waste piles from Douro Coalfield (Portugal): petrological, geochemical and mineralogical characterization. *Int. J. Coal Geol.* 81, 359–372.
- Ribeiro, J., Ferreira da Silva, E., Pinto De Jesus, A., Flores, D., 2011. Petrographic and geochemical characterization of coal waste piles from Douro Coalfield (NW Portugal). *Int. J. Coal Geol.* 87, 226–236.
- Ribeiro, J., Suárez-Ruiz, I., Ward, C.R., Flores, D., 2016. Petrography and mineralogy of self-burning coal wastes from anthracite mining in the El Bierzo Coalfield (NW Spain). *Int. J. Coal Geol.* 154–155, 92–106.
- Sassen, R., 1984. Effects of radiation exposure on indicators of thermal maturity. *Org. Geochem.* 5, 183–186.
- Scalan, R.S., Smith, J.E., 1970. An improved measure of the odd-to-even predominance in the normal alkanes of sediment extracts and petroleum. *Geochim. Cosmochim. Acta* 34, 611–620.
- Schmidt-Collerus, J.J., 1969. Investigation of the relationship between organic matter and uranium deposits – part II. Experimental investigation. US Atomic Commission Open-File Report GJO-9332, p. 192.
- Sheng, C.H., 2007. Char structure characterised by Raman spectroscopy and its correlations with combustion reactivity. *Fuel* 86, 2316–2324.
- Simoneit, B.R.T., 1989. Organic matter of the troposphere-V. Application of molecular marker analysis to biogenic emissions into the troposphere for source reconciliations. *J. Atmos. Chem.* 8, 251–275.
- Simoneit, B.R.T., Bi, X., Orors, D.R., Medeiros, P.M., Sheng, G., Fu, J., 2007. Phenols and hydroxy-PAHs (arylphenols) as tracer for coal smoke particulate matter: source tests and ambient aerosol assessment. *Environ. Sci. Technol.* 41, 7294–7302.
- Singh, A.K., Singh, M.P., Sharma, M., Srivastava, S.K., 2007. Microstructures and microtextures of natural cokes: a study of heat-affected coking coals from the Jharia coalfield, India. *Int. J. Coal Geol.* 71, 153–175.
- Smieja-Król, B., Cuber, S., Rouzaud, J.N., 2009. Multiscale organisation of organic matter associated with gold and uranium minerals in the Witwatersrand basin, South Africa. *Int. J. Coal Geol.* 78, 77–88.
- Smith Jr., D.K., 1984. Uranium mineralogy. In: De Vivo, B., Ippolito, F., Capaldi, G., Simpson, P.R. (Eds.), *Uranium Geochemistry, Mineralogy, Geology, Exploration and Resources*. Institution of Mining and Metallurgy, London, pp. 43–71.
- Stout, S.A., Emsbo-Mattingly, S.-D., 2008. Concentration and character of PAHs and other hydrocarbons in coals of varying rank – implications for environmental studies of soils and sediments containing particulate coal. *Org. Geochem.* 39, 801–819.

- Stracher, G.B., Prakash, A., Sokol, E.V. (Eds.), 2011. *Coal and Peat Fires: A Global Perspective* Vol. 7. Elsevier, Amsterdam.
- Suárez-Ruiz, I., Crelling, J.C., 2008. *Applied Coal Petrology. The Role of Petrology in Coal Utilization*. Elsevier 388 pp.
- Suárez-Ruiz, I., Flores, D., Mendonça Filho, J.G., Hackley, P., 2012. Review and update of the applications of organic petrology: part 2, geological and multidisciplinary applications. *Int. J. Coal Geol.* 98, 73–94.
- Suk, M. (Ed.), 1984. *Geological History of the Territory of the Czech Socialist Republic*. Geological Survey, Prague, and Academia Publishing House, Prague, p. 396.
- Sýkorová, I., Havelcová, M., Klika, Z., Trejtnarová, H., Fojtíková, M., Martinec, P., Šulc, A., 2010. Carbon particles and organic compounds in hard coal waste. In: Drebenstedt, C., Fischer, C., Meyer, U., Jianjun, W., Bing, K. (Eds.), *Latest Developments in Coal Fire Research. Bridging the Science, Economics, and Politics of a Global Disaster. ICCFR2, 19–21 May 2010, dbb Forum Berlin. TU Bergakademie Freiberg, Germany*, pp. 418–419.
- Szalay, A., 1964. Cation exchange properties of humic acids and their importance in geochemical enrichment of UO<sub>2</sub>. *Geochim. Cosmochim. Acta* 28, 1605–1614.
- Taylor, G.H., Teichmüller, M., Davis, A., Diessel, C.F.K., Littke, R., Robert, P., 1998. *Organic Petrology*. Gebrüder Borntraeger, Berlin-Stuttgart, p. 704.
- ten Haven, H.L., de Leeuw, J.W., Rullkötter, J., Sinnighe Damsté, J.S., 1987. Restricted utility of the pristane/phytane ratio as a palaeoenvironmental indicator. *Nature* 330, 641–643.
- Tuinstra, F., Koenig, J.L., 1970. Raman spectrum of graphite. *J. Chem. Phys.* 53, 1126–1131.
- Vleeskens, J., Kwieńska, B., Roos, M., Hamburg, G., 1994. Coke forms in nature and in power utilities. Interpretation with SEM. *Fuel* 73, 816–822.
- Ward, C.R., Warbrooke, P.R., Roberts, F.I., 1989. Geochemical and mineralogical changes in a coal seam due to contact metamorphism, Sydney basin, New South Wales, Australia. *Int. J. Coal Geol.* 11, 105–125.
- Žáček, V., Skála, R., 2015. Mineralogy of burning-coal waste piles in collieries of the Czech Republic. In: Stacher, G.B., Prakash, A., Sokol, E.V. (Eds.), *Coal and Peat Fires: A Global Perspective Case Studies – Coal Fires* vol. 3. Elsevier, Amsterdam, Boston, Heidelberg, London, pp. 109–160.
- Zumberge, J.E., Sigleo, A.C., Nagy, B., 1978. Molecular and elemental analyses of the carbonaceous matter in the gold- and uranium-bearing Vall Reef carbon seams. Witwatersrand sequence. *Miner. Sci. Eng.* 10, 1126–1131.